RESEARCH ARTICLE

Check for updates

Newly synthesized 6-substituted piperazine/phenyl-9-cyclopentyl containing purine nucleobase analogs act as potent anticancer agents and induce apoptosis *via* inhibiting Src in hepatocellular carcinoma cells†

Ebru Bilget Guven, [iD] ‡[ab] Irem Durmaz Sahin,‡[cd] Duygu Altiparmak,[a] Burak Servili, [iD][e] Sebnem Essiz, [iD][be] Rengul Cetin-Atalay[fg] and Meral Tuncbilek*[a]

Newly synthesized 6-substituted piperazine/phenyl-9-cyclopentyl-containing purine nucleobase analogs were tested for their *in vitro* anticancer activity against human cancer cells. Compounds **15**, **17–24**, **49**, and **56** with IC$_{50}$ values less than 10 μM were selected for further examination on an enlarged panel of liver cancer cell lines. Experiments revealed that compound **19** utilizes its high cytotoxic potential (IC$_{50}$ < 5 μM) to induce apoptosis *in vitro*. Compound **19** displayed a KINOMEscan selectivity score S_{35} of 0.02 and S_{10} of 0.01 and demonstrated a significant selectivity against anaplastic lymphoma kinase (ALK) and Bruton's tyrosine kinase (BTK) over other kinases. Compounds **19**, **21**, **22**, **23**, and **56** complexed with ALK, BTK, and (discoidin domain-containing receptor 2) DDR2 were analyzed structurally for binding site interactions and binding affinities *via* molecular docking and molecular dynamics simulations. Compounds **19** and **56** displayed similar interactions with the activation loop of the kinases, while only compound **19** reached toward the multiple subsites of the active site. Cell cycle and signaling pathway analyses exhibited that compound **19** decreases phosho-Src, phospho-Rb, cyclin E, and cdk2 levels in liver cancer cells, eventually inducing apoptosis.

1. Introduction

Cancer cells are mostly known for their unlimited cell proliferation potential and owe this competence to the intricate adaptation of the metabolic pathways in which they are involved. All these rearrangements eventually aim to increase not only the energy but also the synthesis of fundamental substrates – both required for an accelerated proliferation rate.[1,2] Cancer cells foster the *de novo* biosynthesis of purines, the building blocks of nucleic acids, as a precisely reasonable strategy to prosper and spread; therefore, purine analogs offer a formidable pharmacological strategy as an anticancer agent.[3,4]

Despite their toxicities, purine analogs are resourceful therapeutic agents, emphasizing that their selectivity should be improved.[3] Purine analogs are structurally alike and share a straightforward mechanism of action that eventually induces apoptosis.[5] Interestingly, these antimetabolites display a distinguished difference in their biochemical activities and therefore have an expansive potential to constitute a class of therapeutic agents against various diseases.[5,6] Even one atom change in the structure of purine analogs can result in a very different clinical activity, as seen in the two FDA-approved drugs, clofarabine and cladribine.[5,7]

Hepatocellular carcinoma (HCC) is the dominant type of primary liver cancer which is known to be the third leading cause of cancer death worldwide in 2020 and found to be the cancer type with the second-lowest survival rate (18%) for all stages combined.[8,9] Heterogeneity of the HCC mainly

[a] Department of Pharmaceutical Chemistry, Faculty of Pharmacy, Ankara University, 06560, Yenimahalle, Ankara, Turkey.
E-mail: tuncbile@pharmacy.ankara.edu.tr
[b] Department of Molecular Biology and Genetics, Faculty of Engineering and Natural Sciences, Kadir Has University, 34083, Cibali-Fatih, Istanbul, Turkey
[c] Department of Molecular Biology and Genetics, Faculty of Science, Bilkent University, 06800, Bilkent, Ankara, Turkey
[d] School of Medicine, Koc University, 34450, Sarıyer, İstanbul, Turkey
[e] Graduate School of Science and Engineering, Bioinformatics and Genetics Program, Kadir Has University, Fatih 34083, Istanbul, Turkey
[f] Cancer System Biology Laboratory, CanSyL, Graduate School of Informatics, Middle East Technical University, 06800, Ankara, Turkey
[g] Section of Pulmonary and Critical Care Medicine, The University of Chicago, Chicago, IL, 60637, USA
† Electronic supplementary information (ESI) available. See DOI: **https://doi.org/10.1039/d3md00440f**
‡ These authors contributed equally to this work.

depends on rearranged metabolic pathways, which can offer strategies in drug discovery if it is known how these intricately modified pathways give rise to HCC tumor growth.[10] Although there are FDA-approved tyrosine kinase inhibitors as first- and second-line treatment options for advanced HCC patients, they all have limited effects on the survival rates of the patients.[11] Purine metabolism, which has been recently shown to foster HCC tumor development, is unfortunately not known evidently, but it is already appreciated that purine analogs are promising antimetabolites to suppress HCC tumor growth.[12]

The proto-oncogene, c-Src, is a tyrosine kinase that plays a pivotal role in the signal transduction pathways controlling cancer cell growth and proliferation. Increased c-Src kinase activity is a common phenomenon demonstrated in various human tumors.[13,14] c-Src kinase activation triggers the cyclin E–Cdk2 complex to propel the cells in the S-phase through hyper-phosphorylation of retinoblastoma protein, Rb, which assists the transcription factor E2F to get released from Rb and leads the cell cycle progress. Inactivation of c-Src induces apoptosis in liver cancer cells but not in primary hepatocytes. Thus, c-Src should be considered a promising target in anticancer drug discovery.[15,16] Anaplastic lymphoma kinase (ALK) is a receptor tyrosine kinase that initiates a signaling pathway after receiving the extracellular signal. Depending on the mutation ALK contains, a different signaling pathway becomes activated in tumor cells, and c-Src is one of the possible downstream effectors of ALK.[17] Bruton's tyrosine kinase (BTK) is also known to function as an upstream activator of c-Src and, moreover, is determined to be in interaction with ALK.[18,19]

In our previous studies, we have reported important cytotoxic activities of 9-(β-D-ribofuranosyl//4-trifluoromethylbenzyl/4-chlorobenzyl//tetrahydropyran)-6-(4-trifluoromethyl phenylpiperazine/4-phenoxyphenyl)purine analogs (**I**), (**II**), (**III**), (**IV**), and **36** (Fig. 1).[20–23] In the present work, we report the synthesis of new derivatives of purines (**I**), (**II**), (**III**), (**IV**), and **36** as 9-cyclopentyl-purines (**11–24** and **47–56**) and evaluate their cytotoxic effects against human epithelial cancer cells: liver (Huh7), colon (HCT116), and breast (MCF7) (Tables 2 and 3). With the potent analogs **15**, (**17–24**), (**49**), and (**56**), further screening was done against hepatocellular carcinoma (HCC) cell lines Huh7, Hep3B, HepG2, PLC, Mahlavu, FOCUS, Snu475, Snu182, Snu387, Snu398, Snu423, and Snu449 (Table 4). This analysis sheds light on the pathway leading liver cancer cells to apoptosis. Moreover, the possible protein kinase inhibition potential of these newly synthesized purine analogs has been investigated, and it was shown that these compounds might be promising intracellular kinase inhibitors. In order to identify any existing direct interaction with the human kinome, KINOMEscan™ profiling was applied. It is a high-throughput approach based on active site-directed competition binding of the sample to be tested and a selected human kinase list. The KINOMEscan™ analysis evidently demonstrates that among the novel purine analogs, compound **19** selectively interacts with ALK and
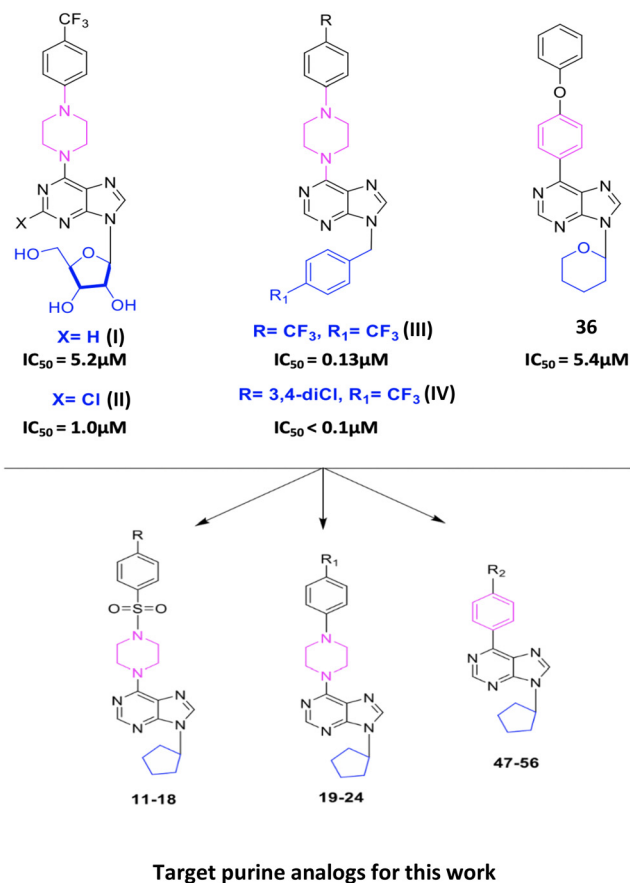

Fig. 1 Structures of 9-(β-D-ribofuranosyl//4-trifluoromethyl/4-chlorobenzyl//tetrahydro-pyran)-6-(4-trifluoromethylphenylpiperazine/4-phenoxyphenyl) purine analogs (**I**), (**II**), (**III**), (**IV**), and **36** and target purine compounds **11–24** and **47–56**.

BTK, while compound **56** interacts with DDR2 (discoidin domain-containing receptor 2). These compounds are examined for binding affinity scores to target kinases by two different molecular docking softwares. The docking poses are further tested with 10 nanosecond molecular dynamics simulations. Molecular interactions of compounds **19** and **56** in the binding site display distinct contacts with the activation loop of the kinases. We have also demonstrated that c-Src inactivation plays a central role in inducing apoptosis for the cancer cells treated with these newly synthesized purine analogs.

2. Results and discussion

The synthesis of 6-(4-substituted phenyl sulfonyl piperazine)-9-cyclopentyl purine analogs (**11–18**) was performed starting from 6-chloropurin (**1**). The nucleophilic substitution of **1** to cyclopentyl bromide afforded the intermediate purine (**2**) under basic conditions.[24] Treatment of the piperazine structure with (4-substituted phenyl)sulfonyl chlorides in CH_2Cl_2 gave the corresponding sulfonylated piperazine derivatives (**3–10**). Compounds **11–18** were obtained by
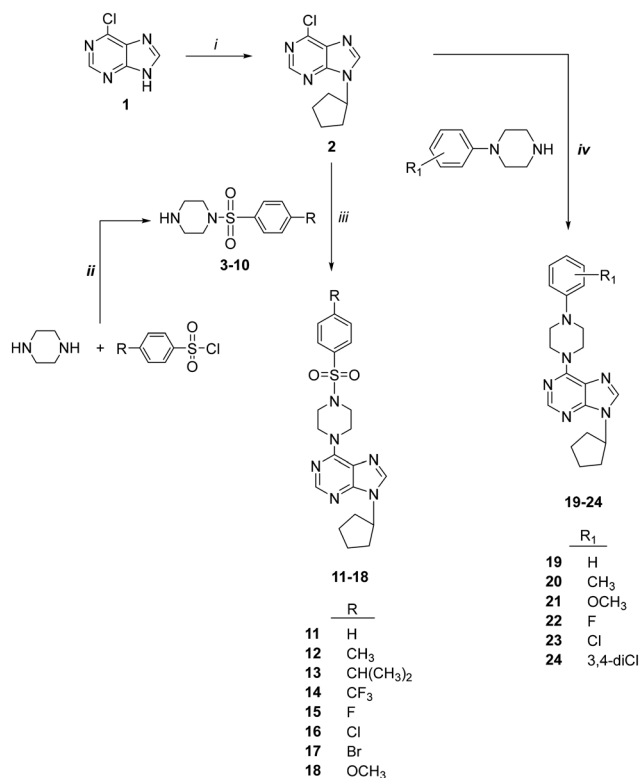
Scheme 1 Synthesis of compounds **11**–**24**. Reagents: (i) cyclopentyl bromide, K_2CO_3, DMSO; (ii) CH_2Cl_2; (iii) Et_3N, EtOH; (iv) 4-substituted piperazines, Et_3N, EtOH.
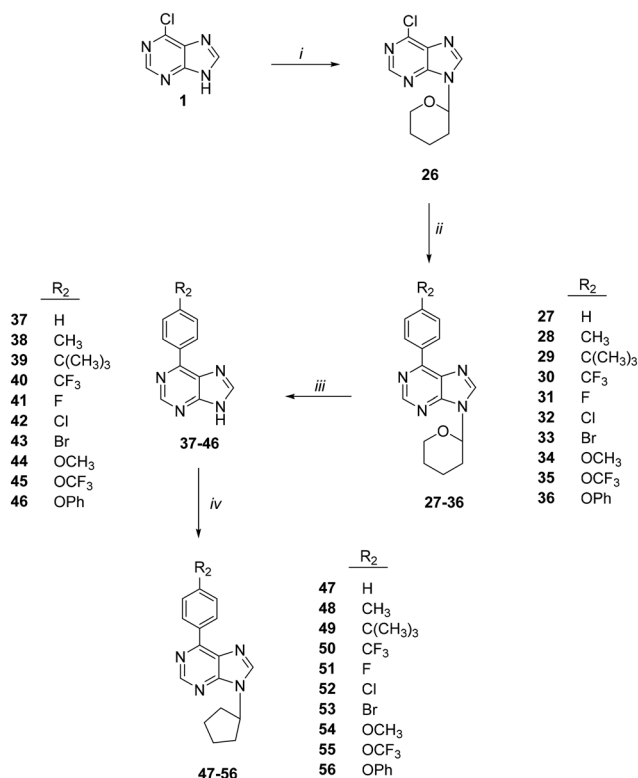
Scheme 2 Synthesis of compounds **47**–**56**. Reagents: (i) cyclopentyl bromide, K_2CO_3, DMSO; (ii) CH_2Cl_2; (iii) Et_3N, EtOH; (iv) 4-substituted piperazines, Et_3N, EtOH.

amination of chlorine of (**2**) with the synthesized piperazines (**3**–**10**) in the presence of a base.

We wondered if removing the sulfonyl group on the piperazine ring could impact the compound's activity. Therefore, we synthesized 6-(4-substituted phenyl piperazine)-9-cyclopentyl purine derivatives (**19**–**24**) from compound **2**. Thus, purines substituted with phenyl piperazines at position C-6 (**19**–**24**) were prepared with the nucleophilic aromatic substitution reaction of **2** with the appropriate piperazines using triethylamine in ethanol (Scheme 1).

The synthesis of 6-(4-substituted phenyl)-9-cyclopentyl purine analogs **47**–**56** from 6-chloropurine (**1**) was performed in four steps (Scheme 2). The N-9 position tetrahydropyran-2-yl (THP) derivative **26** was obtained by the carbocation reaction of compound **1** with 3,4-dihydro-2H-pyran using p-TSA as a catalyst. 6-(Substituted phenyl) purines, **27**–**36**, were prepared by Suzuki coupling reaction. This coupling reaction produced compounds **27**–**36** from 4-substituted phenyl boronic acids in toluene catalyzed by Pd (PPh$_3$)$_4$. The deprotection of the THP group with Dowex 50 X8 (H$^+$) in methanol afforded 6-(4-substituted phenyl) purine **37**–**46** derivatives. Finally, the target compounds **47**–**56** were successfully obtained via N-9 alkylation of **37**–**46** with cyclopentyl bromide in the presence of sodium hydride.

The structures of all compounds were confirmed by ^{1}H, ^{13}C NMR mass spectral data, and elemental analysis.

The *in vitro* cytotoxic activities of the newly synthesized compounds (**11**–**24**) and (**47**–**56**) were initially evaluated against human liver (Huh7), colon (HCT116), and breast (MCF7) cancer cell lines using NCI-sulforhodamine B (SRB) colorimetric assay. Time-dependent IC$_{50}$ values for each compound were calculated in comparison with 5-fluorouracil (5-FU), cladribine, fludarabine, and pentostatine as reference anticancer agents. The results are summarized in Tables 1–3.

The investigation of 6-(4-substituted phenyl sulfonyl piperazine)-9-cyclopentyl purine derivatives (**11**–**18**) for their cytotoxic activities revealed that compounds bearing F (**15**), Br (**17**), and OCH$_3$ (**18**), as a substitution at the phenyl ring, had IC$_{50}$ values of 9 μM, 8 μM, and 7.1 μM respectively on the Huh7 cancer cell line which is much lower when compared to well-known agents 5-FU (IC$_{50}$: 30.7 μM) and fludarabine (IC$_{50}$: 29.9 μM). Compounds **11**, **13**, and **14** (with IC$_{50}$ values in the range of 12.3–14.7 μM) were also more cytotoxic than 5-FU and fludarabine on Huh7 liver cancer cells. On the other hand, compound **17** (IC$_{50}$: 8.4 μM), which contains 4-Br–Ph substitution, showed comparable activities with fludarabine (IC$_{50}$: 8.3 μM) on the HCT116 colon cancer cell line. Compounds **15**, **17**, and **18** (IC$_{50}$: 5.2 μM, 6.5 μM, and 8.6 μM respectively) were also more cytotoxic than fludarabine (IC$_{50}$: 15.2 μM) on the MCF7 breast cancer cell line (Table 1, Fig. 2).

The 6-(4-substituted phenyl piperazine)-9-cyclopentyl purine analogs (**19**–**24**) bearing 4-CF$_3$–Ph, 4-Cl–Ph, 4-(3,4-

Table 1 *In vitro* cytotoxicity of 6-(4-substituted phenyl sulfonyl piperazine)-9-cyclopentyl purine analogs **11**–**18** on different human cancer cell lines (Huh7, HCT116, and MCF7)
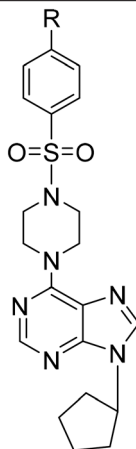
Cancer cell lines, $IC_{50}{}^{a}$ μM

Compound	R	Huh7	HCT116	MCF7
11	H	13.1 ± 5.1	12 ± 4.7	11.2 ± 3.7
12	CH_3	49 ± 11.3	196.6 ± 45.6	170.9 ± 39.3
13	$CH(CH_3)_3$	14.7 ± 2.4	11.5 ± 0.9	17.2 ± 2.1
14	CF_3	12.3 ± 2.5	32.4 ± 9.5	12.7 ± 3.3
15	F	9 ± 2.2	12 ± 1.5	5.2 ± 1.9
16	Cl	34.4 ± 5.7	44.8 ± 9.5	10.5 ± 1.0
17	Br	8 ± 1.2	8.4 ± 1.5	6.5 ± 0.8
18	OCH_3	7.1 ± 2.0	10.4 ± 1.4	8.6 ± 3.5
5-FU		30.7 ± 2.0	6.0 ± 0.2	3.5 ± 0.8
Cladribine		1.3 ± 0.4	<0.1	2 ± 2.0
Fludarabine		29.9 ± 20.0	8.3 ± 3.0	15.2 ± 0.1
Pentostatine		NI	NI	NI

[a] IC_{50} values were calculated from the cell growth inhibition curves obtained from the treatments done with increasing concentrations of each molecule (40 μM, 20 μM, 10 μM, 5 μM, and 2.5 μM) for 72 h. Experiments are done in duplicate. NI: no inhibition.

diCl)–Ph substitution at their piperazine ring (**23**, **24**) showed high bioactivities (IC_{50}: 0.1 μM, 0.1 μM, and 0.04 μM respectively) on the Huh7 liver cancer cell line providing highly promising results. These compounds also showed higher bioactivities than known cytotoxic agents 5-FU, cladribine, fludarabine, and pentostatine. In addition, four other compounds from this group of derivatives, **19**, **20**, **21**, and **22**, came forward with their druggable (<5 μM) IC_{50} values in the range of 1.0–3.8 μM. The compound with the highest cytotoxic activity in this group was compound **24** (IC_{50}: 0.04 μM). The compounds with a non-substituted phenyl group at the piperazine ring, compound **19** (IC_{50}: 0.1 μM) and compounds **21** (IC_{50}: 1 μM) and **24** (IC_{50}: 0.16 μM) showed higher cytotoxic activities than other known agents (5-FU, cladribine, fludarabine, and pentostatine) (Table 2, Fig. 3).

Among the 6-(4-substituted phenyl)-9-cyclopentyl purine analogs (**47**–**56**), the most active compound **56**, which has a 4-OPh–Ph group at the sixth position of the purine ring, was shown to have druggable (<5 μM) IC_{50} values in the range of 0.8–2.8 μM against all three cancer cell lines (Huh7, HCT116, and MCF7) which makes compound **56** much more potent compared to 5-FU, fludarabine, and pentostatine. Besides,

compound **49**, which contains 4-C(CH₃)₃–Ph substitution, also displayed higher cytotoxic activity (IC_{50}: 6.3 μM) than known anticancer agents 5-FU, fludarabine, and pentostatine (Table 3, Fig. 4).

The compounds **15**, (**17**–**24**), **49**, and **56** with IC_{50} values less than 10 μM were selected to be further examined on an enlarged panel of liver cancer cell lines that are Huh7, Hep3B, HepG2, PLC, Mahlavu, FOCUS, Snu475, Snu182, Snu387, Snu398, Snu423, and Snu449. Among the 6-(4-substituted phenyl piperazine)-9-cyclopentyl purine analogs **24** and 6-(4-substituted phenyl)-9-cyclopentyl purine analog **56** displayed remarkable cytotoxicity superior to well-known anticancer agents cladribine and fludarabine on Huh7, HepG2, and Hep3B cell lines. On the other hand, among the same group, compounds **19**, **22**, **24**, **49**, and **56** had significantly better cytotoxicities compared to cladribine and fludarabine on the PLC cell line. Compounds **19**, **24**, and **56** showed high cytotoxic activities on Mahlavu, FOCUS, and Snu475 cell lines as well (Table 4).

Consequently, these results suggested that cytotoxic activity increases remarkably when a directly substituted phenyl group replaces the phenyl sulfonyl substitution to the 4th position of the piperazine ring. Among all the

Table 2 *In vitro* cytotoxicity of 6-(4-substituted phenyl piperazine)-9-cyclopentyl purine analogs (**19–24**) on different human cancer cell lines (Huh7, HCT116, and MCF7)
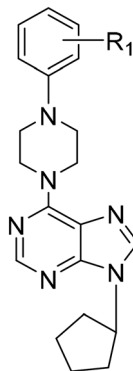
Cancer cell lines, IC_{50}[a] μM

Compound	R_1	Huh7	HCT116	MCF7
19	H	1 ± 0.2	2.1 ± 0.3	0.1 ± 0.1
20	CH_3	1.4 ± 0.1	1.9 ± 0.6	6.4 ± 1.9
21	OCH_3	3.8 ± 0.1	5 ± 2.1	1 ± 0.7
22	F	1.6 ± 0.3	1.6 ± 0.5	9.1 ± 2.3
23	Cl	0.1 ± 0.1	0.6 ± 0.3	4.1 ± 1.1
24	3,4-DiCl	0.04 ± 0.01	0.04 ± 0.03	0.16 ± 0.1
5-FU		30.7 ± 2.0	6.0 ± 0.2	3.5 ± 0.8
Cladribine		1.3 ± 0.4	<0.1	2 ± 2.0
Fludarabine		29.9 ± 20.0	8.3 ± 3.0	15.2 ± 0.1
Pentostatine		NI	NI	NI

[a] IC_{50} values were calculated from the cell growth inhibition curves obtained from the treatments which were done with increasing concentrations of each molecule (40 μM, 20 μM, 10 μM, 5 μM, and 2.5 μM) for 72 h. Experiments were done in duplicate. NI: no inhibition.

synthesized molecules, the most active group corresponds to the group with substituted phenyl piperazine (**19–24**). Moreover, the most active compounds accommodated electrons attracting 4-CF_3, Cl, and 3,4-diCl substitutes in the phenyl ring. Finally, 4-OPh in the compounds with direct phenyl substitution at the 6th position of the purine ring increased cytotoxic activity. Furthermore, the bioactivities of the compounds analyzed on the enlarged panel of liver cancer cell lines, compounds **15**, (**17–24**), **49**, and **56** were further confirmed in real-time *via* a real-time cell electronic sensing (RT-CES) system (Fig. 5). The results obtained confirmed that five of the derivatives in this group, compounds **19**, **21**, **22**, **23**, and **56**, have promising cytotoxic potential against liver cancer cells; therefore, these newly synthesized purine analogs were selected to be further investigated for their mechanism of action on cancer cells.

Human liver cancer cells were treated with 5 μM of the selected compounds **19**, **21**, **22**, **23**, and **56** for 72 h. Hoechst-dye-stained cells' nuclei were observed under a fluorescence microscope. As seen in Fig. 6, the cell morphologies of the treated cells compared to DMSO-negative controls were distinctive. Treatment with the compounds resulted in condensed nuclei with a horseshoe-like structure indicating apoptotic induction.

Cell cycle analysis was performed to elucidate further the effect of compounds **19**, **21**, **22**, **23**, and **56** on the liver cancer cells. Huh7 and Mahlavu liver cancer cells were treated with

5 μM of the compounds. The DNA content of the cells was stained with propidium iodide (PI) and analyzed through a flow cytometer. Analysis of the results suggested a significant increase in the SubG1 phase of the cells treated with the research compounds. These results also suggest the induction of apoptosis in the presence of selected compounds (Fig. 7).

Considering that the results of the cell cycle analysis support the previous observation of the morphological changes, which suggested the induction of apoptosis in cancer cells treated with compounds **19**, **21**, **22**, **23**, and **56**, we first investigated the cleavage of the apoptosis marker poly ADP-ribosyl polymerase PARP-1 protein with western blot analysis. Huh7 liver cancer cells were treated with 5 μM of these selected compounds for 72 h and then analyzed with western blot to characterize the cell death type. The obtained large apoptotic fragment (89 kDa) pointed out that all four compounds induced PARP-1 cleavage, confirming the induction of the programmed cell death mechanism in liver cancer cells (Fig. 8).

The literature showed that a group of novel purine derivatives could inhibit c-Src kinase.[25] Therefore, the activity levels of c-Src kinases were first investigated to find the mechanism of action of our novel nucleobase and nucleoside analogs. For this purpose, Huh7 cells were treated with 5 μM of the six compounds for 72 h and then analyzed with western blot using specific antibodies for c-Src kinase and its

Table 3 *In vitro* cytotoxicity of 6-(4-substituted phenyl)-9-cyclopentyl purine analogs (**47**–**56**) on different human cancer cell lines (Huh7, HCT116, and MCF7)
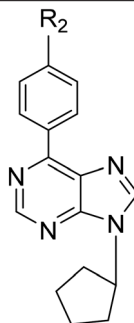
Cancer cell lines, IC_{50}[a] µM

Compound	R_2	Huh7	HCT116	MCF7
47	H	12.8 ± 3.1	13.9 ± 2.9	15.7 ± 1.2
48	CH_3	23.8 ± 7.2	22.4 ± 1.7	17.7 ± 3.1
49	$C(CH_3)_3$	6.3 ± 1.1	6.6 ± 0.4	12.6 ± 1.1
50	CF_3	29.8 ± 1.9	6 ± 1.3	20.3 ± 4.2
51	F	6.7 ± 0.9	6.1 ± 0.9	15.6 ± 2.7
52	Cl	15.6 ± 3.5	NI	NI
53	Br	16 ± 2.1	NI	56.1 ± 8.2
54	OCH_3	10.6 ± 0.9	39 ± 7.4	19.5 ± 2.3
55	OCF_3	15.1 ± 1.3	26.3 ± 8.8	24 ± 1.5
56	OPh	1.2 ± 0.3	0.8 ± 0.1	2.8 ± 0.3
5-FU		30.7 ± 2.0	6.0 ± 0.2	3.5 ± 0.8
Cladribine		1.3 ± 0.4	<0.1	2 ± 2.0
Fludarabine		29.9 ± 20.0	8.3 ± 3.0	15.2 ± 0.1
Pentostatine		NI	NI	NI

[a] IC_{50} values were calculated from the cell growth inhibition curves obtained from the treatments which were done with increasing concentrations of each molecule (40 µM, 20 µM, 10 µM, 5 µM, and 2.5 µM) for 72 h. Experiments were done in duplicate. NI: no inhibition.

active phosphorylated form. Our data demonstrated that treatment with compounds **19** and **23** resulted in a significant decrease in the levels of phospho-Src, meaning that these purine analogs inhibit the activation of Src protein (Fig. 8). Moreover, the downstream elements of the Src pathway were also investigated.[26] We observed that compound **19** decreased the expression of the phospho-Rb levels, which means that the Rb protein is activated in these samples. Likewise, the expression levels of cyclin E and cdk2 were also decreased in cancer cells treated with compound **19** compared to its corresponding DMSO control (Fig. 8).

The newly synthesized nucleobase and nucleoside analogs were suspected of having kinase inhibitory activity based on similar previous findings in the literature. Therefore, we performed a kinase assay with these molecules. Human liver cancer (Huh7 and Mahlavu) cells were treated with 5 µM of these compounds for 72 h. Afterward, the effect of the compounds on ATP levels was detected using the Lonza Kinase Glo Plus luminescence kit. Multikinase inhibitor staurospourine was used as the positive control of the assay.

Results revealed that all the compounds except **19** did not affect the intracellular ATP levels indicating that they do not have any kinase inhibitory effects (Fig. 9). However, compound **19** showed a considerable increase in luminescence, indicating high ATP levels, which indirectly

may suggest that compound **19** might be inhibiting intracellular kinases.

The reasonable suspicion for compound **19** to be a putative kinase inhibitor stimulated us to figure out any possible direct interaction of the newly synthesized purine analogs with the human kinome. KINOMEscan™ profiling, a high-throughput approach based on active site-directed competition binding of the sample to be tested and the selected list of human kinases, was preferred to investigate any direct interaction, if existing, of compound **19** with the human kinome. KINOMEscan™ profiling service reported that the 6-(4-substituted phenyl piperazine)-9-cyclopentyl purine analog, compound **19**, interacted with anaplastic lymphoma kinase (ALK) and Bruton's tyrosine kinase (BTK) while compound **56** interacts with DDR2 (discoidin domain-containing receptor 2). Selectivity scores S_{35} of 0.02 and S_{10} of 0.01 were reported for compound **19**, while the selectivity scores S_{35} of 0.01 and S_{10} of 0.01 were reported for compound **56** (Fig. 10).

The results obtained from KINOMEscan™ were further explored with *in silico* techniques to understand the structural interactions of the test compounds with suggested kinases. Mainly, test compounds **19**, **21**, **22**, **23**, and **56** were docked to ALK, BTK, and DDR2 together with the reference molecules, cladribine, fludarabine, 5-FU, pentostatin, and STR. The
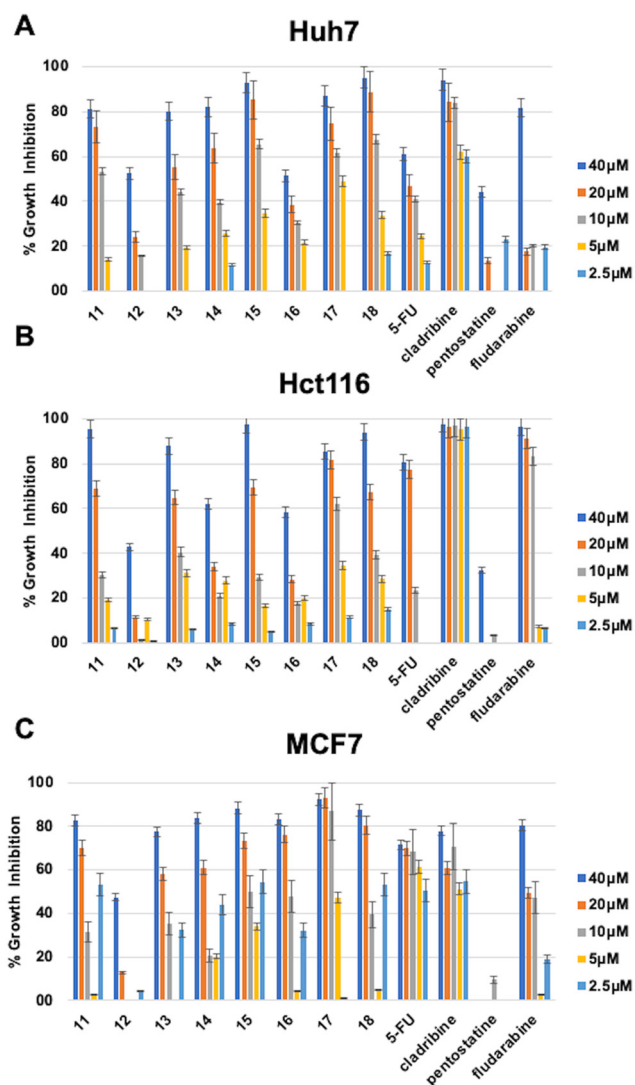
Fig. 2 Percentage growth inhibition of compounds **11**–**18** on (A) Huh7 liver cancer, (B) Hct116 colon cancer, and (C) MCF7 breast cancer cell lines. In order to investigate their growth inhibitory effect, Huh7 liver cancer cells were treated with the compounds for 72 h in triplicate with decreasing concentrations (40 μM, 20 μM, 10 μM, 5 μM, and 2.5 μM). NCI-SRB analysis was performed to investigate the effect of the compounds on cellular growth. DMSO was used as a negative control. Percentage growth inhibitions were calculated by normalizing to the DMSO control.

Fig. 3 Percentage growth inhibition of compounds **19**–**24** on (A) Huh7 liver cancer, (B) Hct116 colon cancer, and (C) MCF7 breast cancer cell lines. In order to investigate their growth inhibitory effect, Huh7 liver cancer cells were treated with the compounds for 72 h in triplicate with decreasing concentrations (40 μM, 20 μM, 10 μM, 5 μM, and 2.5 μM). NCI-SRB analysis was performed to investigate the effect of the compounds on cellular growth. DMSO was used as a negative control. Percentage growth inhibitions were calculated by normalizing to the DMSO control.

binding affinities are displayed in Table 5, together with the PDB codes used for the target kinases which are 5P9J,[27] 5FTO,[28] and 7AYM.[29] The docking poses from AutoDock Vina were cross-checked with the results of SwissDock. Docked poses generated by AutoDock Vina were all in agreement with the poses generated by SwissDock, and one representative result, the docking poses of compound **19** from SwissDock and AutoDock Vina with BTK, ALK, and DDR2, is displayed in Fig. S1.† In the Table S1,† the binding affinity scores from SwissDock is also displayed along with AutoDock Vina scores. This cross-checking step is essential in demonstrating the accuracy of the molecular docking results.
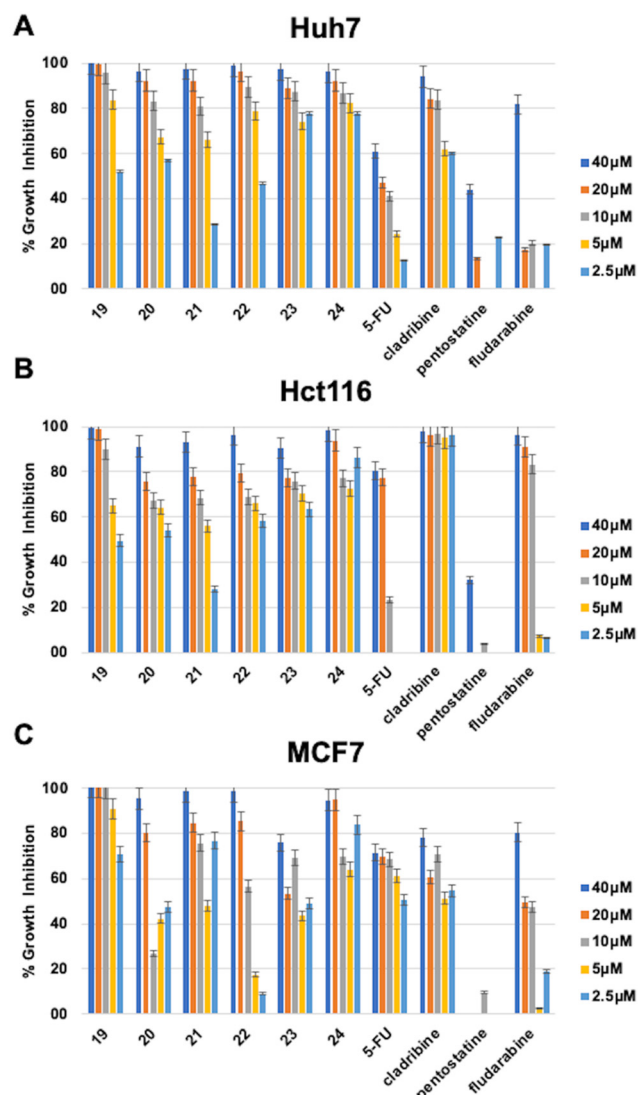
Considering the binding energy values given in Table 5, all the test compounds, **19** to **56**, give better binding energies than the reference molecules, which are known to be non-kinase inhibitors. This agrees with the results of KINOMEscan™. Namely, the purine analogs filtered and selected through multiple steps in this study are effective inhibitor candidates for BTK, ALK, and DDR2 proteins. The affinities of the best-docked compounds ranged between −7.4 kcal mol^{-1} and −10.3 kcal mol^{-1} (Table 5). One other significant result observed in Table 5, our purine analog molecules all displayed similar or better binding energies than STR, a well-known, broad-spectrum kinase inhibitor.[30,31]
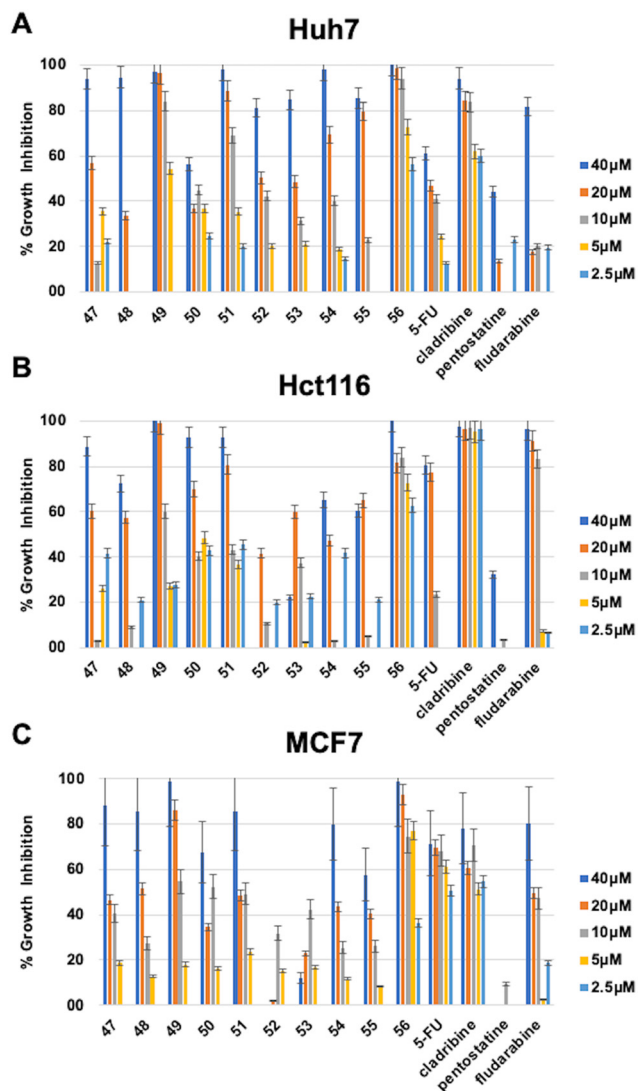
Fig. 4 Percentage growth inhibition of compounds 47–56 on (A) Huh7 liver cancer, (B) Hct116 colon cancer, and (C) MCF7 breast cancer cell lines. In order to investigate their growth inhibitory effect, Huh7 liver cancer cells were treated with the compounds for 72 h in triplicate with decreasing concentrations (40 μM, 20 μM, 10 μM, 5 μM, and 2.5 μM). NCI-SRB analysis was performed to investigate the effect of the compounds on cellular growth. DMSO was used as a negative control. Percentage growth inhibitions were calculated by normalizing to the DMSO control.

Although compounds 19 and 56 displayed good binding affinities in general, to understand the structural features and interactions of the target molecules, we studied the compounds' binding poses. Before studying the binding pockets and its interactions, one final step has been taken for ensuring the binding poses obtained from the molecular docking step. Namely 10 ns solvated molecular dynamics simulations were carried with compound 19 docked at BTK, compound 19 docked at ALK, and compound 56 docked at DDR2. Fig. 11A displays all-atom RMSD values of the compounds in the binding pocket. RMSD values are all around 1.5 to 2 Ångstroms while the

RMSD of compound 56 in DDR2 stayed even as low as 1 Ångstrom. Furthermore the change in the binding poses at the end of simulation is compared with the initial poses visually in Fig. 11B–D. As it is clear from the figure (initial pose shown in green and final pose in gray), the docking pose remained very similar to the initial position. After ensuring the binding pose with two different docking softwares and all-atom MD simulations, the poses obtained are analyzed further.

Since the kinase inhibitors are thoroughly studied and well categorized according to how they access different regions of the binding site, the known structural features of kinase binding sites should be summarized before going into the details of the binding site interactions.[32] The binding pockets of kinases are divided into the front cleft, back cleft, and gate area, which has a gatekeeper region regulating substrate access to the active site of the kinase (different regions are displayed with different colors in Fig. 12A). For instance, Type I$\frac{1}{2}$ inhibitors, such as lapatinib and lenvatinib, can pass the gatekeeper and access the back pocket of kinases, while Type II inhibitors occupy the front pocket and gate area but cannot reach the back pocket, such as axitinib and dabrafenib.[33] A critical activation loop also moves away from the ATP-binding site and forms a beta-hairpin conformation for substrate binding.[32]

The compounds in this study all targeted three main subsites on BTK, the front and back cleft, as well as the gate area around the ATP-binding site. This makes them like Type I$\frac{1}{2}$ inhibitors (Fig. 12B and C). However, the main difference between compounds 21, 22, and 23 (Fig. 12C) and compounds 19 and 56 (Fig. 12B) is around a hydrophobic interaction with an amino acid of the activation loop (Leu542). Table S1† summarizes the important interactions between the target molecules and the kinase-binding site residues. Although compounds 21, 22, and 23 reached the back pocket of the BTK active site, no interaction with the activation loop was observed (Fig. 12C). Only compounds 19 and 56 interacted with this loop (Fig. 12B), mainly resulting in a possible lock-down of the activation loop to move away from the ATP-binding site. This is an important site where a conformational change in the activation loop leads to the formation of a β-hairpin for substrate binding in a functioning state of the enzyme.[32,34]

When ALK and DDR2 interactions are considered, compounds 19, 21, 22, 23, and 56 compounds were docked on the main front pocket of the ALK and DDR2 active sites. Again, in Fig. 13, the pose of compound 19 was displayed with three different target kinases superimposed. In ALK, the molecule reached the front pocket and gate area but could not reach the back pocket, and in DDR2, it entered from the back pocket and the gate area. Only in BTK it extended over the front and back pockets, and the gatekeeper residue L1196. Again, compound 19 displayed the most extended blockage in the binding site; thus, observing the best inhibition results with compound 19 in the previous sections is rational.

Table 4 IC_{50} values of compounds **15**, **(17–24)**, **(49)**, and **(56)** against hepatocellular carcinoma (HCC) cell lines: Huh7, Hep3B, HepG2, PLC, Mahlavu, FOCUS, Snu475, Snu182, Snu387, Snu398, Snu423, and Snu449

HCC cell line, $IC_{50}{}^a$ μM					
Compound	Huh7	Hep3B	HepG2	PLC	Mahlavu	FOCUS
15	9 ± 1.3	6.1 ± 2.5	4.8 ± 1.9	15.4 ± 5.7	11.4 ± 2.5	12.6 ± 3.5
17	9.1 ± 1.7	4.3 ± 1.0	6.3 ± 0.2	9.2 ± 1.1	20.5 ± 3.2	15.9 ± 5.1
18	17 ± 0.8	71.8 ± 14.8	2.7 ± 0.4	84.6 ± 31.1	9 ± 1.2	10.1 ± 2.7
19	3 ± 0.4	<0.1	2.4 ± 1.5	4 ± 0.5	0.2 ± 0.1	0.6 ± 0.3
20	2.9 ± 0.4	3.1 ± 0.7	0.9 ± 0.5	20.7 ± 2.3	4.2 ± 1.3	5 ± 1.1
21	1.3 ± 1.3	0.3 ± 0.1	0.3 ± 0.1	9.3 ± 1.4	0.6 ± 1.2	2.6 ± 1.4
22	1.5 ± 0.1	4.3 ± 0.2	0.5 ± 0.2	6 ± 1.8	7 ± 0.1	1.5 ± 0.7
23	1.7 ± 0.9	0.4 ± 0.2	0.01 ± 0.01	19.3 ± 3.5	4 ± 2.0	2 ± 0.3
24	0.4 ± 0.2	0.03 ± 0.01	0.02 ± 0.01	7 ± 2.7	0.1 ± 0.1	0.5 ± 0.3
49	8.1 ± 2.3	6.7 ± 1.7	2.7 ± 0.2	3.4 ± 0.4	4 ± 0.4	2 ± 0.6
56	0.7 ± 0.2	0.1 ± 0.1	0.002 ± 0.001	6.5 ± 0.9	0.1 ± 0.01	0.5 ± 0.2
Cladribine	0.6 ± 0.2	0.1 ± 0.1	0.4 ± 0.1	9.1 ± 1.6	<0.1	<0.1
Fludarabine	24.4 ± 5.4	27.8 ± 3.3	17 ± 1.8	41.7 ± 5.3	14.2 ± 0.9	13.7 ± 1.6

HCC cell line, $IC_{50}{}^a$ μM					
Compound	Snu475	Snu182	Snu387	Snu398	Snu423	Snu449
15	21.6 ± 4.4	47.9 ± 7.3	11.1 ± 2.5	8 ± 1.7	9.5 ± 2.2	16.3 ± 5.5
17	9 ± 2.7	60.6 ± 9.4	15.9 ± 2.1	4 ± 0.9	10.5 ± 2.1	8.5 ± 2.1
18	57.5 ± 13.1	NI	15.8 ± 1.7	6.9 ± 2.2	6.8 ± 0.9	20 ± 3.9
19	5.8 ± 1.1	6 ± 1.5	13 ± 1.8	1.2 ± 0.1	11 ± 1.7	2 ± 0.3
20	17.7 ± 3.8	61 ± 10.4	88 ± 13.2	1.9 ± 0.5	17.5 ± 2.3	17 ± 2.7
21	13 ± 0.4	13 ± 3.9	38 ± 12.7	0.3 ± 0.1	15 ± 3.3	2 ± 0.9
22	7 ± 1.2	41 ± 8.4	26 ± 7.4	1 ± 0.4	16 ± 1.5	3.3 ± 1.1
23	12.3 ± 3.4	12.2 ± 1.3	2 ± 0.9	1.8 ± 1.0	4 ± 0.5	6.9 ± 2.1
24	2.5 ± 1.1	65 ± 10.3	20 ± 3.7	0.2 ± 0.1	9.9 ± 0.7	<0.1
49	12.3 ± 2.5	12.2 ± 1.4	2 ± 0.5	1.8 ± 0.2	4 ± 1.2	6.9 ± 0.7
56	2.5 ± 0.8	65 ± 10.4	20 ± 3.7	0.2 ± 0.1	9.9 ± 0.9	<0.1
Cladribine	2.5 ± 1.1	23.3 ± 7.2	7.1 ± 2.9	<0.1	6.7 ± 1.1	37.3 ± 8.2
Fludarabine	41.5 ± 4.3	37.2 ± 2.1	33.8 ± 8.6	0.2 ± 0.1	32.6 ± 4.6	25.1 ± 4.7

^{a} IC_{50} values were calculated from the cell growth inhibition curves obtained from the treatments, which were done with increasing concentrations of each molecule (40 μM, 20 μM, 10 μM, 5 μM, and 2.5 μM) for 72 h. Experiments were done in triplicate. NI: no inhibition.

3. Experimental

3.1 Chemistry

Melting points were recorded with a capillary melting point apparatus (Electrothermal 9100) and were uncorrected. NMR spectra were recorded on a VARIAN Mercury 400 FT-NMR spectrometer (400 for ^{1}H, 100.6 MHz for ^{13}C). TMS was used as an internal standard for the ^{1}H and ^{13}C NMR spectra; δ values are given in ppm and J values are in Hz. Mass spectra were taken on a Waters Micromass ZQ by using the (ESI+) method. Elemental analyses (C, H, N) were determined on a Leco CHNS 932 instrument and values within ±0.4% of the theoretical values were obtained. Column chromatography was accomplished on silica gel 60 (0.040–0.063 mm particle size). The chemical reagents used in synthesis were purchased from E. Merck, Fluka, Sigma, and Aldrich. Compounds **3–10**,[35–38] **26**, **27**, **29–33**,[23] **34**,[39] **36**, **37**,[23] **38**,[40] **39–43**,[23] **44**,[39] and **46** (ref. 23) were prepared according to the literature methods.

3.1.1 General procedure for the synthesis of sulfonate compounds (11–18). 6-Chloro-9-cyclopentyl-9H-purine (**2**) (1 mmol)[20] was dissolved in 5 mL absolute EtOH, then (4-substituted phenyl)sulfonyl piperazines (1 mmol) and (Et)$_3$N (3 mmol) were added. The mixture was refluxed for 18–24 h. The reaction mixture was concentrated *in vacuo*, and the residue was purified by column chromatography (EtOAc–hexane, 2 : 1).

6-[4-(Phenyl sulfonyl)piperazine-1-yl]-9-cyclopentyl-9H-purine (11). Yield 61.9%; mp 152–155 °C. ^{1}H NMR (CDCl$_3$) δ 1.74–2.00 (m, 6H), 2.20–2.32 (m, 2H), 3.16 (t, 4H), 4.45 (br s, 4H), 4.88–4.98 (m, 1H), 7.52 (t, 2H), 7.58 (t, 1H), 7.75 (s, 1H), 7.78 (d, 2H), 8.32 (s, 1H). ^{13}C NMR (CDCl$_3$) δ 23.77, 32.67, 44.36, 46.18, 55.74, 120.23, 127.77, 129.13, 132.99, 135.36, 136.82, 151.11, 151.94, 153.35. MS (ESI+) *m/z*: 413.2 (100%) (M + H)$^+$. Anal. calcd for $C_{20}H_{24}N_6O_2S \cdot 0.3CH_3COOC_2H_5 \cdot 0.01H_2O$: C, 58.01; H, 6.02; N, 19.15; S, 7.29. Found C, 58.46; H, 6.07; N, 18.77; S, 7.22.

6-[4-(4-Methylphenylsulfonyl)piperazine-1-yl]-9-cyclopentyl-9H-purine (12). Yield 75.5%; mp 181–183 °C. ^{1}H NMR (CDCl$_3$) δ 1.74–2.0 (m, 6H), 2.20–2.31 (m, 2H), 2.39 (s, 3H), 3.13 (t, 4H), 4.43 (br s, 4H), 4.87–4.98 (m, 1H), 7.30 (d, 2H, J_o = 8 Hz), 7.64 (d, 2H, J_o = 8.4 Hz), 7.77 (s, 1H), 8.31 (s, 1H). ^{13}C NMR (CDCl$_3$) δ 21.50, 23.78, 32.69, 44.57, 46.18, 55.85, 120.14, 127.83, 129.75, 132.27, 136.94, 143.91, 150.88, 151.51, 152.88. MS (ESI+) *m/z*: 427.1 (100%) (M + H)$^+$. Anal. calcd for $C_{21}H_{26}N_6O_2S$: C, 59.13; H, 6.14; N, 19.70; S, 7.52. Found C, 59.12; H, 6.33; N, 19.36; S, 7.56.
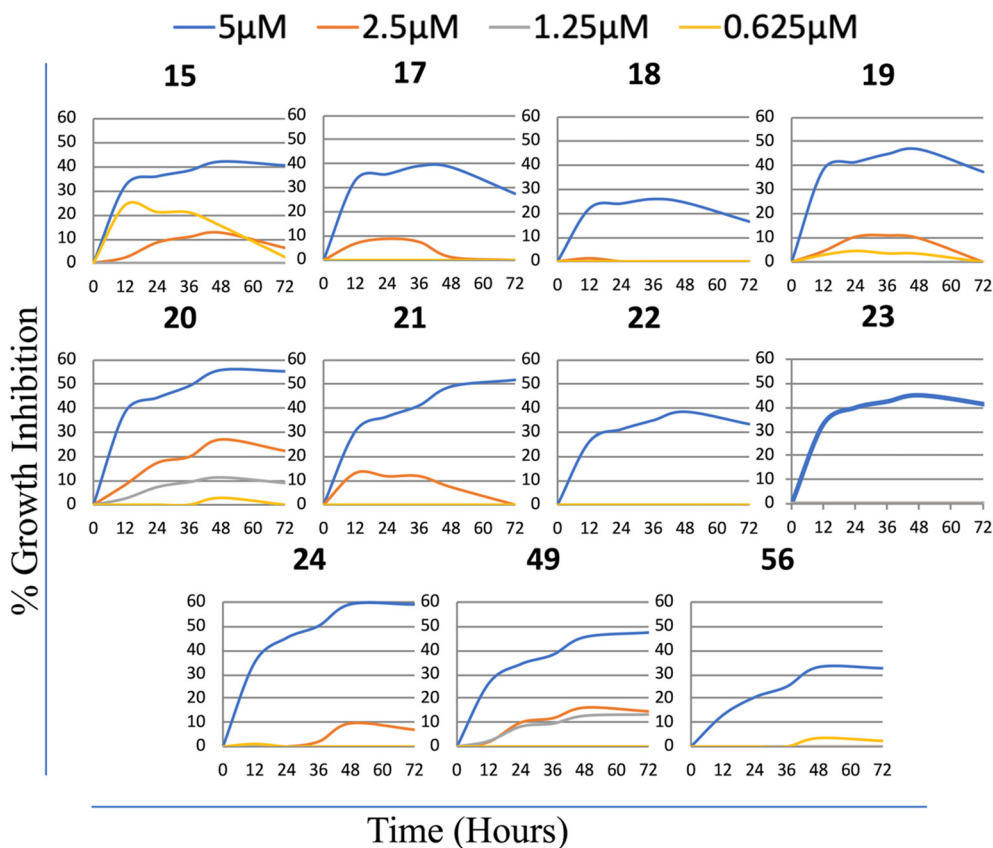
Fig. 5 Real-time cell analysis of Huh7 treated with the selected compounds. Cells were treated with the selected compounds and observed in real-time with RT-CES. In order to analyze their real-time growth inhibitory effects on Huh7 cells DMSO was used as a negative control. The plots corresponding to each concentration were normalized, considering the data obtained from the DMSO-treated cells. The experiment was performed in triplicate.
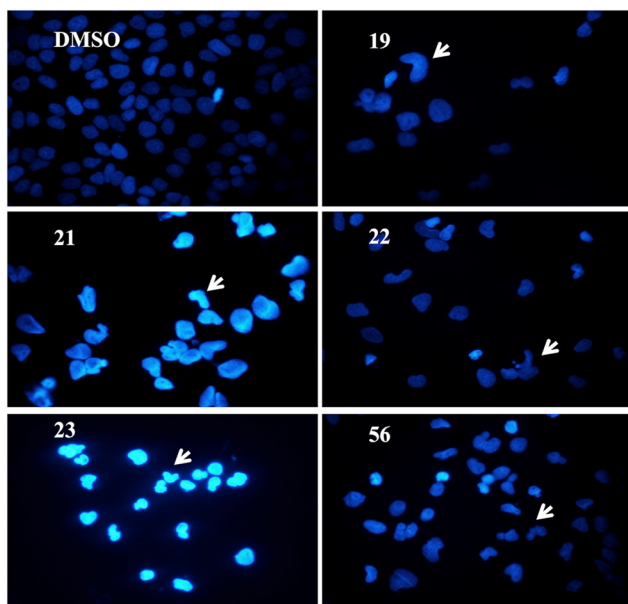

Fig. 6 Morphological changes induced by the compounds **19**, **21**, **22**, **23**, and **56**. In order to visualize the alteration, Huh7 liver cancer cells were treated with 5 μM of the compounds for 72 h and stained with Hoechst 33258 dye. Images were taken with a 40× objective lens.

6-[4-(4-Isopropylphenylsulfonyl)piperazine-1-yl]-9-cyclopentyl-9H-purine (13). Yield 76.6%; mp 165–168 °C. ^{1}H NMR (CDCl$_3$) δ 1.24 (d, 3H), 1.29 (d, 3H), 1.72–1.98 (m, 6H), 2.20–2.31 (m, 2H), 2.90–3.03 (m, 1H), 3.07–3.20 (t, 5H), 4.44 (br s, 4H), 4.87–4.96 (m, 1H), 7.35 (d, 2H, J_o = 8 Hz), 7.67 (d, 2H, J_o = 8.4 Hz), 7.78 (s, 1H), 8.32 (s, 1H). ^{13}C NMR (CDCl$_3$) δ 23.57, 23.60, 23.76, 32.65, 34.13, 44.35, 46.18, 55.72, 120.21, 127.19, 127.96, 132.63, 136.77, 151.11, 151.95, 153.36, 154.47. MS (ESI+) *m/z*: 455.3 (100%) (M + H)$^+$. Anal. calcd for C$_{23}$H$_{30}$N$_6$O$_2$S: C, 60.77; H, 6.65; N, 18.49; S, 7.05. Found C, 60.68; H, 6.44; N, 18.35; S, 7.12.

6-[4-[4-(Trifluoromethyl)phenylsulfonyl]piperazine-1-yl]-9-cyclopentyl-9H-purine (14). Yield 85.6%; mp 205–208 °C. ^{1}H NMR (CDCl$_3$) δ 1.74–1.98 (m, 6H), 2.20–2.30 (m, 2H), 3.18 (t, 4H), 4.46 (br s, 4H), 4.88–4.96 (m, 1H), 7.79 (d, 3H), 7.89 (d, 2H, J_o = 7.6 Hz), 8.32 (s, 1H). ^{13}C NMR (CDCl$_3$) δ 23.77, 32.67, 44.34, 46.13, 55.77, 120.26, 123.11 (q, J = 271.2 Hz), 126.32 (q, J = 3.8 Hz), 128.23, 134.71 (q, J = 32.7 Hz), 136.92, 139.17, 151.16, 151.94, 153.27. MS (ESI+) *m/z*: 481.2 (100%) (M + H)$^+$. Anal. calcd for C$_{21}$H$_{25}$F$_3$N$_6$O$_2$S: C, 52.49; H, 4.82; N, 17.49; S, 6.67. Found C, 52.31; H, 4.53; N, 17.27; S, 6.74.

6-[4-(4-Fluorophenylsulfonyl)piperazine-1-yl]-9-cyclopentyl-9H-purine (15). Yield 96.4%; mp 154–157 °C. ^{1}H NMR (CDCl$_3$) δ 1.74–2.0 (m, 6H), 2.20–2.30 (m, 2H), 3.14 (t, 4H), 4.45 (br s,
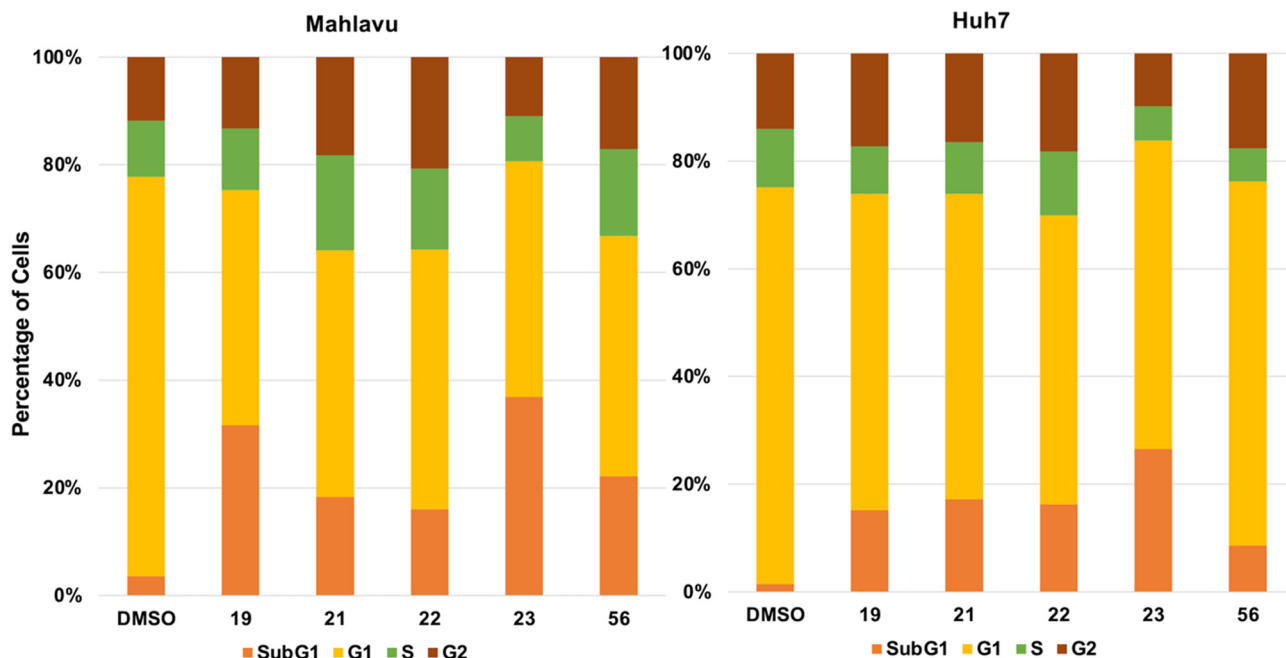
Fig. 7 Cell cycle arrest induced by selected compounds. Huh7 and Mahlavu liver cancer cells were treated with 5 μM of the compounds. The DNA within the cells was stained using propidium iodide (PI) and subsequently evaluated using a flow cytometer. The analysis of the findings indicated a noteworthy elevation in the SubG1 phase among the cells subjected to the experimental compounds. These outcomes additionally hint at the initiation of apoptosis in the presence of the chosen substances.

4H), 4.89–4.97 (m, 1H), 7.19 (t, 2H), 7.76–7.79 (m, 3H), 8.32 (s, 1H). ^{13}C NMR (CDCl$_3$) δ 23.77, 32.67, 44.34, 46.15, 55.75, 116.44 (d, J = 22.5 Hz), 120.25, 130.50 (d, J = 9.6 Hz), 131.42, 136.87, 151.13, 151.95, 153.31, 165.32 (d, J = 253.9 Hz). MS (ESI+) m/z: 431.1 (100%) (M + H)$^+$. Anal. calcd for
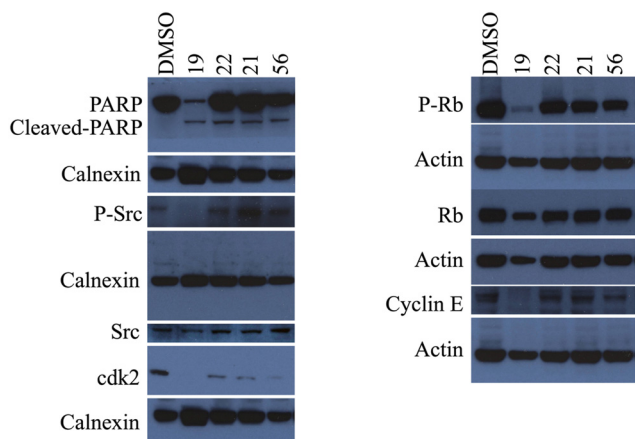

Fig. 8 Cellular pathway components targeted by the selected six compounds. Huh7 cells were treated with 5 μM of the compounds **19**, **21**, **22**, **23**, and **56** for 72 h. Western blot analysis showed that PARP is cleaved confirming induction of apoptosis. Furthermore, compounds **19** and **23** induced a significant decrease in the levels of phospho-Src, suggesting the inhibition of Src protein. Compound **19** decreased the expression of the phospho-Rb levels, thereby activated Rb protein. In addition, levels of cyclin E and cdk2 were also decreased in cancer cells treated with compound **19** compared to its corresponding DMSO control.
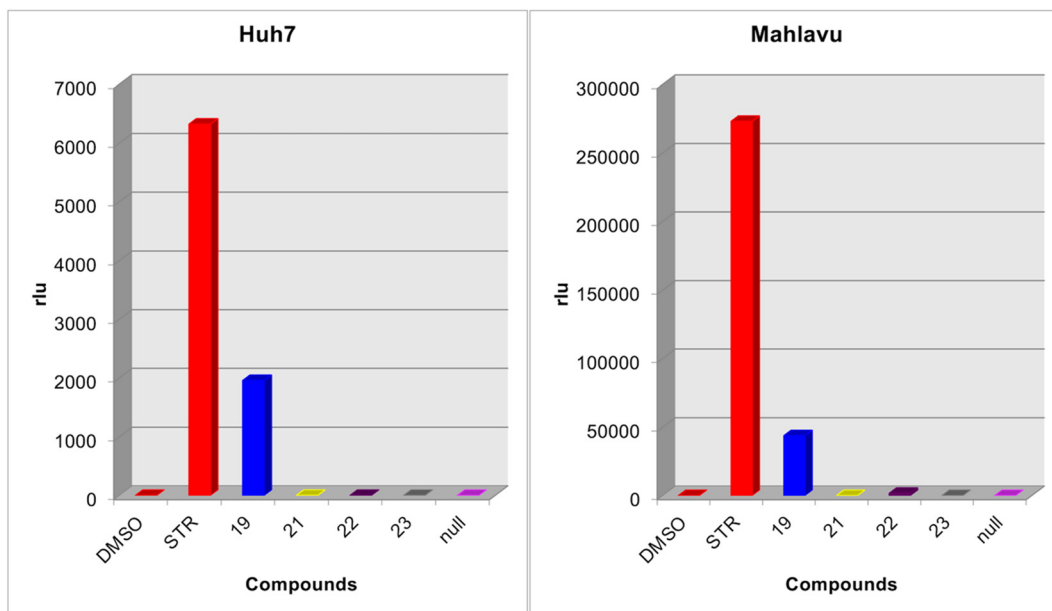
C$_{20}$H$_{23}$FN$_6$O$_2$S: C, 55.80; H, 5.39; N, 19.52; S, 7.45. Found C, 55.84; H, 5.38; N, 19.08; S, 7.44.

6-[4-(4-Chlorophenylsulfonyl)piperazine-1-yl]-9-cyclopentyl-9H-purine (16). Yield 53.9%; mp 171–175 °C. ^{1}H NMR (CDCl$_3$) δ 1.75–2.0 (m, 6H), 2.20–2.32 (m, 2H), 3.15 (t, 4H), 4.46 (br s, 4H), 4.88–4.99 (m, 1H), 7.49 (d, 2H, J_o = 8.4 Hz), 7.69 (d, 2H, J_o = 8 Hz), 7.78 (s, 1H), 8.33 (s, 1H). ^{13}C NMR (CDCl$_3$) δ 23.77, 32.66, 44.33, 46.12, 55.75, 120.26, 129.14, 129.45, 133.92, 136.86, 139.64, 151.14, 151.93, 153.30. MS (ESI+) m/z: 447.2 (100%) (M + H)$^+$. Anal. calcd for C$_{20}$H$_{23}$ClN$_6$O$_2$S·0.3H$_2$O: C, 53.10; H, 5.26; N, 18.58; S, 7.09. Found C, 53.23; H, 5.25; N, 18.21; S, 7.34.

6-[4-(4-Bromophenylsulfonyl)piperazine-1-yl]-9-cyclopentyl-9H-purine (17). Yield 94.9%; mp 176–179 °C. ^{1}H NMR (CDCl$_3$) δ 1.74–1.99 (m, 6H), 2.20–2.31 (m, 2H), 3.14 (t, 4H), 4.45 (br s, 4H), 4.89–4.97 (m, 1H), 7.63 (q, 4H), 7.79 (s, 1H), 8.33 (s, 1H). ^{13}C NMR (CDCl$_3$) δ 23.77, 32.66, 44.35, 46.12, 55.75, 120.26, 128.14, 129.22, 132.44, 134.44, 136.86, 151.15, 151.94, 153.30. MS (ESI+) m/z: 491.2 (98%) (M$^+$), 493.2 (100%) (M + 2)$^+$. Anal. calcd for C$_{20}$H$_{23}$BrN$_6$O$_2$S·0.13C$_6$H$_{14}$: C, 49.66; H, 4.97; N, 16.72; S, 6.38. Found C, 49.43; H, 5.01; N, 16.33; S, 6.46.

6-[4-(4-Methoxyphenylsulfonyl)piperazine-1-yl]-9-cyclopentyl-9H-purine (18). Yield 91.8%; mp 137–140 °C. ^{1}H NMR (CDCl$_3$) δ 1.73–1.99 (m, 6H), 2.21–2.31 (m, 2H), 3.13 (t, 4H), 3.84 (s, 3H), 4.44 (br s, 4H), 4.89–4.96 (m, 1H), 6.96 (d, 2H, J_o = 8.8 Hz), 7.69 (d, 2H, J_o = 8.8 Hz), 7.78 (s, 1H), 8.32 (s, 1H). ^{13}C NMR (CDCl$_3$) δ 23.76, 32.66, 44.32, 46.19, 55.58, 55.72, 114.27, 120.21, 126.80, 129.91, 136.76, 151.09, 151.95, 153.34, 163.14. MS (ESI+) m/z: 443.3 (100%) (M + H)$^+$. Anal. calcd for C$_{21}$H$_{26}$N$_6$O$_3$S: C, 57.0; H, 5.92; N, 18.99; S, 7.25. Found C, 56.77; H, 5.84; N, 18.8; S, 7.35.

Fig. 9 Kinase inhibition potential of the selected compounds. Huh7 and Mahlavu cells were treated with 5 μM of compounds **19**, **21**, **22**, **23**, and **56** or DMSO control. Then, the Lonza Kinase Glo luminescence kit was applied to observe the kinase activity in the cell samples after being treated with the compounds. The relative light units (rlu) for each tested sample are presented in bar graphs.
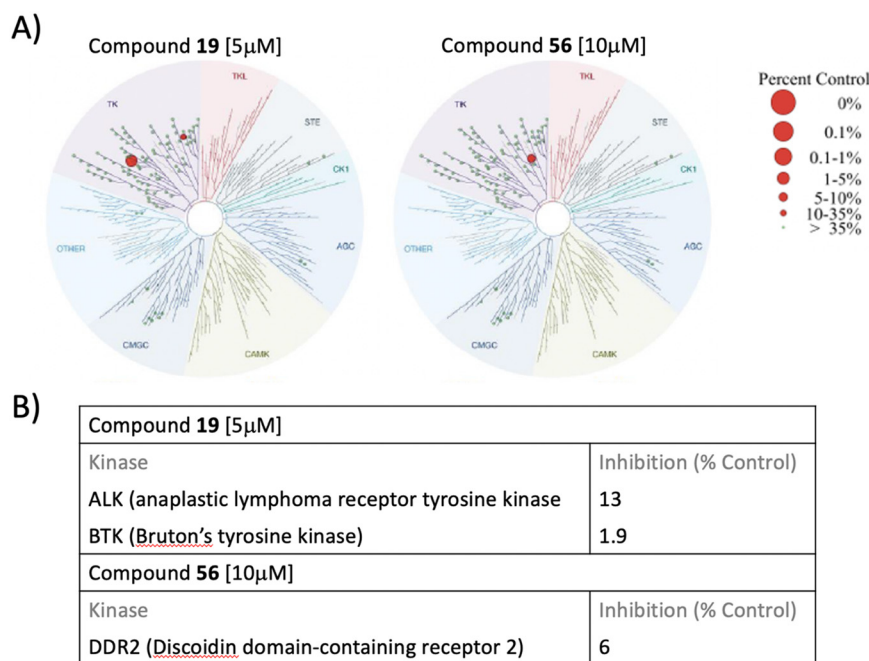

Compound **19** [5μM]	
Kinase	Inhibition (% Control)
ALK (anaplastic lymphoma receptor tyrosine kinase	13
BTK (Bruton's tyrosine kinase)	1.9
Compound **56** [10μM]	
Kinase	Inhibition (% Control)
DDR2 (Discoidin domain-containing receptor 2)	6

Fig. 10 Kinases were selected by compounds **19** and **56**. (A) TREE*spot*™ kinase interaction mapping for compound **19** at a concentration of 5000 nM and compound **56** at a concentration of 10 000 nM. (B) The list of the kinases and their corresponding interaction affinities.

3.1.2 General procedure for the synthesis of compounds 19–24. 6-Chloro-9-cyclopentyl-9*H*-purine (**2**) (1 mmol)[20] was dissolved in 5 mL absolute EtOH, then substituted phenyl piperazines (1 mmol) and (Et)$_3$N (3 mmol) were added. The mixture was refluxed for 30–48 h. The reaction mixture was concentrated *in vacuo*, and the residue was purified by column chromatography (EtOAc–hexane, 2:1).

6-(4-Phenylpiperazine-1-yl)-9-cyclopentyl-9H-purine **(19)**. Yield 88%; mp 99–102 °C. ^{1}H NMR (CDCl$_3$) δ 1.76–2.03 (m, 6H), 2.24–2.35 (m, 2H), 3.35 (t, 4H), 4.52 (br s, 4H), 4.92–5.01 (m, 1H), 6.80–7.06 (m, 4H), 7.31 (t, 1H), 7.84 (s, 1H), 8.41 (s, 1H). ^{13}C NMR (CDCl$_3$) δ 23.80, 32.70, 45.04, 49.60, 55.68, 116.48, 120.22, 120.35, 129.19, 136.52, 151.06, 151.26, 152.12, 153.83. MS (ESI+) *m/z*: 349.4 (100%) (M + H)$^+$. Anal. calcd for

Table 5 Binding affinities of AutoDock Vina

Compound	Affinity (kcal mol^{-1})		
	BTK/5P9J	ALK/5FTO	DDR2/7AYM
19	−9.2	−9.1	−8.9
21	−8.3	−8.4	−7.4
22	−9.3	−9.1	−9.0
23	−9.1	−8.6	−8.8
56	−10.3	−8.9	−9.8
Cladribine	−6.8	−6.9	−6.7
Fludarabine	−6.9	−6.4	−6.5
5-FU	−5.0	−4.8	−4.7
Pentostatin	−6.5	−6.8	−6.3
STR	−9.7	−8.6	−7.7

$C_{20}H_{24}N_6 \cdot 0.3H_2O$: C, 67.88; H, 7.01; N, 23.75. Found C, 67.72; H, 7.02; N, 23.58.

6-[4-(4-Methylphenyl)piperazine-1-yl]-9-cyclopentyl-9H-purine (20). Yield 95.9%; mp 142.146 °C. ^{1}H NMR (CDCl$_3$) δ 1.78–2.03 (m, 6H), 2.29 (s, 1H), 2.24–2.35 (m, 2H), 3.29 (t, 4H), 4.51 (br s, 4H), 4.92–5.0 (m, 1H), 6.93 (d, 2H), 7.12 (d, 1H), 7.82 (s, 1H), 8.39 (s, 1H). ^{13}C NMR (CDCl$_3$) δ 20.43, 23.79, 32.70, 45.06, 50.19, 55.66, 116.87, 120.34, 129.71, 129.82, 136.47, 149.18, 151.05, 152.11, 153.82. MS (ESI+) *m/z*: 363.4 (100%) (M + H)$^+$. Anal. calcd for $C_{21}H_{26}N_6 \cdot 0.1H_2O$: C, 69.24; H, 7.25; N, 23.07. Found C, 69.10; H, 6.85; N,22.98.

6-[4-(4-Methoxyphenyl)piperazine-1-yl]-9-cyclopentyl-9H-purine (21). Yield 85.1%; mp 107–110 °C. ^{1}H NMR (CDCl$_3$) δ 1.75–2.04 (m, 6H), 2.2–2.34 (m, 2H), 3.23 (t, 4H), 3.78 (s, 3H), 4.49 (br s, 4H), 4.41–5.0 (m, 1H), 6.87 (d, 2H), 6.92–7.02 (br m, 2H), 7.82 (s, 1H), 8.39 (s, 1H). ^{13}C NMR (CDCl$_3$) δ 23.79, 32.70, 45.19, 51.13, 55.54, 55.66, 114.49, 118.72, 120.34, 136.47, 145.62, 151.05, 152.11, 153.83, 154.19. MS (ESI+) *m/z*: 379.4 (100%) (M + H)$^+$. Anal. calcd for $C_{21}H_{26}N_6O$: C, 66.64; H, 6.92; N, 22.21. Found C, 66.73; H, 7.11; N, 21.83.

6-[4-(4-Fluorophenyl)piperazine-1-yl]-9-cyclopentyl-9H-purine (22). Yield 95.1%; mp 106.5–109 °C. ^{1}H NMR (CDCl$_3$) δ 1.77–2.03 (m, 6H), 2.25–2.36 (m, 2H), 3.26 (t, 4H), 4.52 (br s, 4H), 4.94–5.02 (m, 1H), 6.92–7.04 (m, 4H), 7.84 (s, 1H), 8.41 (s, 1H). ^{13}C NMR (CDCl$_3$) δ 23.79, 32.70, 45.06, 50.63, 55.68, 115.62 (d, *J* = 22.4 Hz), 118.35 (d, *J* = 7.7 Hz), 120.36, 136.55, 147.95, 151.08, 152.10, 153.81, 157.46 (d, *J* = 237.9 Hz). MS (ESI+) *m/z*: 367.4 (100%) (M + H)$^+$. Anal. calcd for $C_{20}H_{23}FN_6 \cdot 0.05H_2O$: C, 65.39; H, 6.34; N, 22.88. Found C, 65.14; H, 5.97; N, 22.76.

6-[4-(4-Chlorophenyl)piperazine-1-yl]-9-cyclopentyl-9H-purine (23). Yield 97.5%; mp 142–144 °C. ^{1}H NMR (CDCl$_3$) δ 1.75–2.04 (m, 6H), 2.22–2.34 (m, 2H), 3.42 (t, 4H), 4.48 (br s, 4H), 4.91–4.99 (m, 1H), 6.98 (d, 2H), 7.51 (d, 2H), 7.82 (s, 1H), 8.39 (s, 1H). ^{13}C NMR (CDCl$_3$) δ 23.79, 32.72, 44.88, 49.57, 55.69, 117.66, 120.34, 125.08, 129.05, 136.61, 149.86, 151.06, 152.09,
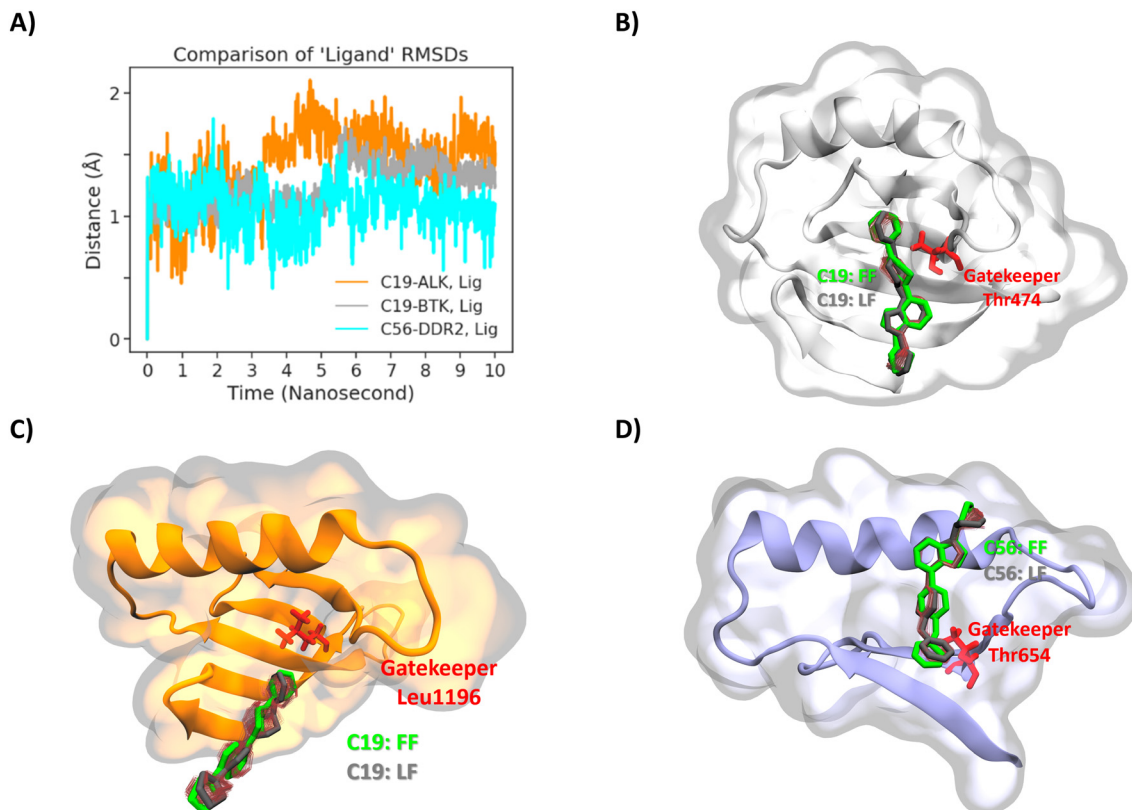

Fig. 11 A) RMSD analysis of the ligands C19 (ALK, BTK) and C56 (DDR2) (A). Compound **19** on the BTK (B), ALK (C), and compound **56** on the DDR2 (D) were visualized to compare the first (FF) and last frame (LF) poses. The red scratches around the compounds show all motion of the compounds over 10 nanoseconds. The green and gray colors indicate the compounds' first and last frame poses in the active kinase sites. The red-colored licorice represents the gatekeepers.
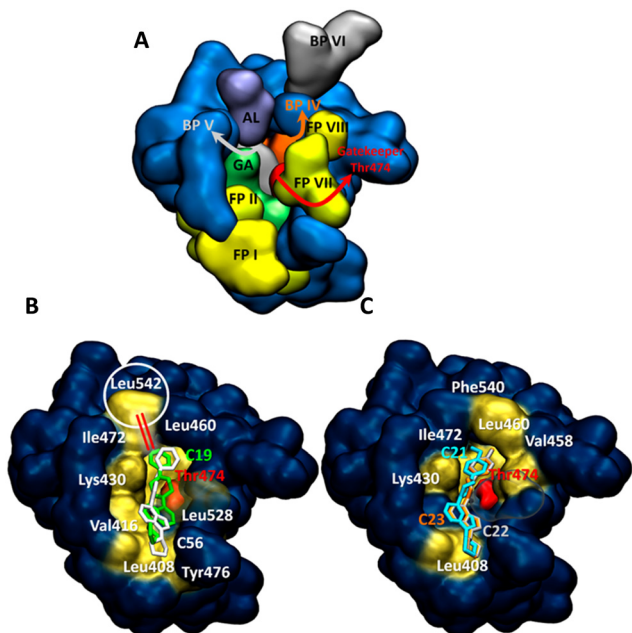
Fig. 12 Binding site analysis: inhibitor interactions in BTK of the active site (A). Hydrophobic interactions are shown in yellow. (B) Compounds **19** and **56** in the binding site. (C) Compounds **21**, **22** and **23** in the binding site. GK: gatekeeper, FC: front cleft, BC: back cleft, FP: front pocket, BP: back pocket, GA: gate area, AL: activation loop.
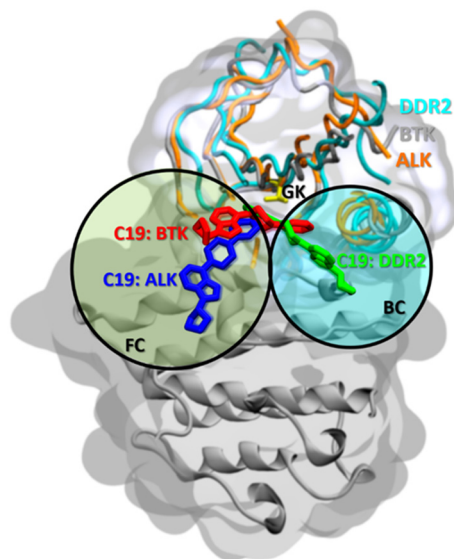

Fig. 13 Binding poses of compound **19** with BTK, ALK, and DDR2. Protein structures are superimposed, and compound **19** is shown in different colors in licorice representation. The yellow color shows the gatekeeper (GK). FC: front cleft, BC: back cleft.

153.75. MS (ESI+) *m/z*: 383.3 (100%) (M + H)⁺, 385.9 (15%) (M + H + 2)⁺. Anal. calcd for $C_{20}H_{23}ClN_6$: C, 62.74; H, 6.05; N, 21.95. Found C, 62.83; H, 6.01; N, 21. 21.66.

6-[4-(3,4-Dichlorophenyl)piperazine-1-yl]-9-cyclopentyl-9H-purine (24). Yield 75.6%; mp 122–125 °C. ¹H NMR (CDCl₃) δ 1.80–2.04 (m, 6H), 2.30–2.45 (m, 2H), 3.44 (t, 4H), 4.58 (br s,

4H), 5.02–5.16 (m, 1H), 6.81 (d, 1H), 7.02 (s, 1H), 7.34 (d, 1H, J_o = 8.8 Hz), 7.99 (s, 1H), 8.59 (s, 1H). ¹³C NMR (CDCl₃) δ 23.88, 33.01, 47.81, 49.01, 57.23, 115.90, 117.88, 119.20, 123.75, 130.75, 133.09, 139.28, 145.55, 149.46. MS (ESI+) *m/z*: 417.3 (100%) (M⁺), 419.3 (82%) (M + 2)⁺, 421.3 (17%) (M + 4)⁺. Anal. calcd for $C_{20}H_{22}Cl_2N_6$: C, 57.56; H, 5.31; N, 20.14. Found C, 57.67; H, 5.43; N, 20.03.

3.1.3 General procedure for Suzuki coupling reaction (27–36). 6-Chloro-9-(tetrahydropyran-2-yl)-9*H*-purine (**26**) (3 mmol) was dissolved in 20 ml toluene, then K₂CO₃ (6 mmol), 4-substituted phenylboronic acid (6 mmol) and Pd(Ph₃)₄ (0.15 mmol) were added. The mixture was refluxed for 20–46 h. The mixture was refluxed for 30–48 h. The reaction mixture was concentrated *in vacuo*, and the residue was purified by column chromatography (EtOAc–hexane, 1:3).

6-(4-Methylphenyl)-9-(tetrahydro-2H-pyran-2-yl)-9H-purine (28). Yield 23.4%; mp 180–185 °C. ¹H NMR (CDCl₃) δ 1.66–1.85 (m, 3H), 2.05–2.19 (m, 3H), 2.44 (s, 3H), 3.82 (td, *J* = 2.8 Hz, *J* = 11.6 Hz, 1H), 4.21 (d, 1H), 5.85 (dd, *J* = 2.8 Hz, *J* = 10 Hz, 1H), 7.37 (d, *J* = 8.4 Hz, 2H), 8.32 (s, 1H), 8.68 (d, *J* = 8.4 Hz, 2H), 9.0 (s, 1H). ¹³C NMR (CDCl₃) δ 21.62, 22.83, 24.89, 31.85, 68.89, 81.92, 129.44, 129.73, 130.91, 132.88, 141.44, 141.78, 151.59, 152.40, 155.05. MS (ESI+) *m/z*: 211.3 (100%) (M + H-THP)⁺, 295.4 (77%) (M + H)⁺. Anal. calcd for $C_{17}H_{18}N_4O$: C, 69.37; H, 6.16; N, 19.03. Found C, 69.51; H, 6.47; N, 18.68.

6-(4-Trifluoromethoxyphenyl)-9-(tetrahydro-2H-pyran-2-yl)-9H-purine (35). Yield 23.4%; mp 142–144 °C. ¹H NMR (CDCl₃) δ 1.66–1.88 (m, 3H), 2.04–2.22 (m, 3H), 3.83 (td,1H), 4.21 (dm, 1H), 5.86 (dd, 1H), 7.40 (d, 2H), 8.35 (s, 1H), 8.87 (d, 2H), 9.03 (s, 1H). ¹³C NMR (CDCl₃) δ 22.79, 24.86, 31.86, 68.93, 82.02, 120.44 (q, *J* = 256.5 Hz), 120.74, 131.05, 131.50, 134.13, 142.32, 151.18, 151.80, 152.40, 153.35. MS (ESI+) *m/z*: 281.2 (100%) (M + H-THP)⁺, 365.2 (80%) (M + H)⁺. Anal. calcd for $C_{17}H_{15}F_3N_4O_2$: C, 56.04; H, 4.15; N, 15.38. Found C, 56.33; H, 4.41; N, 15.72.

3.1.4 General procedure for the deprotection reaction (37–46). The protected compounds (1 mmol) (**27–36**), Dowex 50 X8 (H⁺) (700 mg), MeOH (10 ml), and H₂O (1 ml) were refluxed. Then the reaction mixture was filtered and washed with saturated methanolic NH₃ and MeOH. The filtrate was evaporated *in vacuo* and recrystallized from EtOAc–hexane.

6-(4-Trifluoromethoxyphenyl)-9H-purine (45). Yield 74.9%; mp 257–259 °C. ¹H NMR (DMSO-d₆) δ 7.59 (d, 2H, *J* = 8.8 Hz), 8.68 (s, 1H), 8.95 (d, 2H, *J* = 8.8 Hz), 8.96 (s, 1H). ¹³C NMR (DMSO-d₆) δ 119.97 (q, *J* = 255.2 Hz), 120.87, 123.80, 131.22, 134.64, 145.31, 149.92, 150.33, 151.75, 153.78. MS (ESI+) *m/z*: 281.2 (100%) (M + H)⁺. Anal. calcd for $C_{12}H_7F_3N_4O$: C, 51.44; H, 2.52; N, 19.99. Found C, 51.79; H, 2.71; N, 19.66.

3.1.5 General procedure for the synthesis of target compounds (47–56). To a suspension of compounds **37–46** (1 mmol) in 5 mL of DMSO, K₂CO₃ (1.2 mmol) and cyclopentyl bromide (1.6 mmol) were added. The reaction mixture was stirred at room temperature for 40–48 h. The reaction mixture was treated with H₂O and extracted with EtOAc. The

extract was dried over Na_2SO_4, the solvent was evaporated *in vacuo*, and the residue was purified by column chromatography (EtOAc–hexane, 1 : 2).

6-Phenyl-9-cyclopentyl-9H-purine (47). Yield 30%; mp 92–94.5 °C. ^1H NMR (CDCl$_3$) δ 1.80–2.13 (m, 6H), 2.30–2.42 (m, 2H), 5.03–5.09 (m, 1H), 7.51–7.60 (m, 3H), 8.17 (s, 1H), 8.77 (d, 2H), 8.03 (s, 1H). ^{13}C NMR (CDCl$_3$) δ 23.89, 32.65, 56.13, 128.66, 129.73, 130.88, 131.49, 135.79, 142.56, 152.09, 152.53, 154.81. MS (ESI+) *m/z*: 265.3 (100%) (M + H)$^+$. Anal. calcd for $C_{16}H_{16}N_4$·0.1H_2O: C, 72.21; H, 6.13; N, 21.05. Found C, 72.34; H, 5.78; N, 20.76.

6-(4-Methylphenyl)-9-cyclopentyl-9H-purine (48). Yield 53.5%; mp 103–106 °C. ^1H NMR (CDCl$_3$) δ 1.78–2.12 (m, 6H), 2.28–2.40 (m, 2H), 2.45 (s, 3H), 5.01–5.09 (m, 1H), 7.37 (d, 2H, J_o = 8.4 Hz), 8.15 (s, 1H), 7.69 (d, 2H, J_o = 8 Hz), 8.99 (s, 1H). ^{13}C NMR (CDCl$_3$) δ 21.61, 23.88, 32.65, 56.08, 129.42, 129.67, 131.27, 133.04, 141.29, 142.29, 152.06, 152.42, 154.85. MS (ESI+) *m/z*: 279.3 (100%) (M + H)$^+$. Anal. calcd for $C_{17}H_{18}N_4$·0.1C_6H_{14}·0.2H_2O: C, 72.75; H, 6.88; N, 19.28. Found C, 73.01; H, 6.62; N, 18.90.

6-(4-t-Butylphenyl)-9-cyclopentyl-9H-purine (49). Yield 73.2%; mp 113–115 °C. ^1H NMR (CDCl$_3$) δ 1.38 (s, 9H), 1.80–2.13 (m, 6H), 2.30–2.40 (m, 2H), 5.01–5.09 (m, 1H), 7.58 (d, 2H, J_o = 8.4 Hz), 8.15 (s, 1H), 8.68 (d, 2H, J_o = 8.4 Hz), 9.0 (s, 1H). ^{13}C NMR (CDCl$_3$) δ 23.89, 31.21, 32.65, 34.93, 56.08, 125.66, 129.48, 131.37, 132.99, 142.33, 152.11, 152.38, 154.23, 154.95. MS (ESI+) *m/z*: 321.4 (100%) (M + H)$^+$. Anal. calcd for $C_{20}H_{24}N_4$: C, 74.97; H, 7.55; N, 17.48. Found C, 75.30; H, 7.72; N, 17.32.

6-(4-Trifluoromethylphenyl)-9-cyclopentyl-9H-purine (50). Yield 43%; mp 137–140 °C. ^1H NMR (CDCl$_3$) δ 1.81–2.24 (m, 6H), 2.32–2.42 (m, 2H), 5.04–5.11 (m, 1H), 7.81 (d, 2H, J_o = 8 Hz), 8.20 (s, 1H), 8.92 (d, 2H, J_o = 7.6 Hz), 9.05 (s, 1H). ^{13}C NMR (CDCl$_3$) δ 23.90, 32.65, 56.30, 122.69, 125.39, 125.51 (q, J = 3.9 Hz), 130.03, 131.74, 132.28 (q, J = 32.1 Hz), 138.99, 143.23, 152.02, 152.85. MS (ESI+) *m/z*: 333.3 (100%) (M + H)$^+$. Anal. calcd for $C_{17}H_{15}F_3N_4$·0.15CH_2Cl_2·0.01C_6H_{14}: C, 59.75; H, 4.49; N, 16.19. Found C, 60.11; H, 4.14; N, 15.82.

6-(4-Fluorophenyl)-9-cyclopentyl-9H-purine (51). Yield 71.5%; mp 119–122 °C. ^1H NMR (CDCl$_3$) δ 1.81–2.12 (m, 6H), 2.32–2.40 (m, 2H), 5.02–5.09 (m, 1H), 7.24 (t, 2H), 8.16 (s, 1H), 8.83–8.87 (m, 2H), 8.99 (s, 1H). ^{13}C NMR (CDCl$_3$) δ 23.89, 32.65, 56.16, 115.69 (d, J = 21.8 Hz), 131.20, 131.93 (d, J = 8.3 Hz), 132.01, 142.57, 152.04, 152.54, 153.56, 164.57 (d, J = 250.1 Hz). MS (ESI+) *m/z*: 283.3 (100%) (M + H)$^+$. Anal. calcd for $C_{16}H_{15}FN_4$·0.1H_2O: C, 67.64; H, 5.39; N, 19.71. Found C, 67.52; H, 5.46; N, 19.41.

6-(4-Chlorophenyl)-9-cyclopentyl-9H-purine (52). Yield 77.2%; mp 159–162 °C. ^1H NMR (CDCl$_3$) δ 1.80–2.12 (m, 6H), 2.30–2.40 (m, 2H), 5.02–5.10 (m, 1H), 7.53 (d, 2H, J_o = 8.4 Hz), 8.17 (s, 1H), 8.78 (d, 2H, J_o = 8.8 Hz), 9.0 (s, 1H). ^{13}C NMR (CDCl$_3$) δ 23.88, 32.63, 56.18, 128.86, 131.04, 131.35, 134.27, 137.10, 142.66, 152.02, 152.62, 153.35. MS (ESI+) *m/z*: 299.3 (100%) (M + H)$^+$, 301.3 (55%) (M + H + 2)$^+$. Anal. calcd for $C_{16}H_{15}ClN_4$: C, 64.32; H, 5.06; N, 18.75. Found C, 64.39; H, 5.14; N, 18.52.

6-(4-Bromophenyl)-9-cyclopentyl-9H-purine (53). Yield 33%; mp 152–155 °C. ^1H NMR (CDCl$_3$) δ 1.82–2.12 (m, 6H), 2.31–2.40 (m, 2H), 5.0–5.09 (m, 1H), 7.69 (d, 2H, J_o = 8 Hz), 8.18 (s, 1H), 8.71 (d, 2H, J_o = 8.8 Hz), 9.0 (s, 1H). ^{13}C NMR (CDCl$_3$) δ 23.88, 32.63, 56.19, 125.71, 131.25, 131.36, 131.84, 134.71, 142.69, 152.02, 152.64, 153.41. MS (ESI+) *m/z*: 343.2 (100%) (M), 345.2 (99%) (M + H + 2). Anal. calcd for $C_{16}H_{15}BrN_4$: C, 55.99; H, 4.41; N, 16.32. Found C, 56.34; H, 4.53; N, 15.93.

6-(4-Methoxyphenyl)-9-cyclopentyl-9H-purine (54). Yield 30.2%; mp 101–104 °C. ^1H NMR (CDCl$_3$) δ 1.80–2.13 (m, 6H), 2.29–2.40 (m, 2H), 3.90 (s, 3H), 5.01–5.09 (m, 1H), 7.08 (d, 2H, J = 8.8 Hz), 8.15 (s, 1H), 8.80 (d, 2H, J = 8.8 Hz), 8.97 (s, 1H). ^{13}C NMR (CDCl$_3$) δ 23.89, 32.67, 55.40, 56.04, 114.06, 128.43, 130.91, 131.47, 142.05, 152.04, 152.31, 154.43, 161.93. MS (ESI+) *m/z*: 295.3 (100%) (M + H)$^+$. Anal. calcd for $C_{17}H_{18}N_4O$·0.2CH_2Cl_2·0.15C_6H_{14}: C, 67.04; H, 6.37; N, 17.28. Found C, 66.90; H, 6.04; N, 17.39.

6-(4-Trifluoromethoxyphenyl)-9-cyclopentyl-9H-purine (55). Yield 75.3%; mp 109–112 °C. ^1H NMR (CDCl$_3$) δ 1.81–2.14 (m, 6H), 2.30–2.42 (m, 2H), 5.02–5.10 (m, 1H), 7.39 (d, 2H, J_o = 8 Hz), 8.18 (s, 1H), 8.86 (d, 2H, J_o = 9.2 Hz), 9.02 (s, 1H). ^{13}C NMR (CDCl$_3$) δ 23.88, 32.63, 56.21, 120.44 (q, J = 255.8 Hz), 120.70, 131.42, 134.31, 142.79, 151.09, 152.05, 152.65, 153.13. MS (ESI+) *m/z*: 349.2 (100%) (M + H). Anal. calcd for $C_{17}H_{15}F_3N_4O$·0.1H_2O: C, 58.32; H, 4.37; N, 16.0. Found C, 58.28; H, 4.18; N, 15.75.

6-(4-Phenoxyphenyl)-9-cyclopentyl-9H-purine (56). Yield 98.4%; mp 112–114 °C. ^1H NMR (CDCl$_3$) δ 1.80–2.13 (m, 6H), 2.31–2.40 (m, 2H), 5.01–5.09 (m, 1H), 7.10 (d, 2H, J = 7.6 Hz), 7.14–7.18 (m, 3H), 7.38 (t, 2H), 8.15 (s, 1H), 8.79 (d, 2H, J = 9.2 Hz), 8.99 (s, 1H). ^{13}C NMR (CDCl$_3$) δ 23.91, 32.66, 56.12, 118.31, 119.63, 123.92, 129.88, 130.61, 131.13, 131.58, 142.31, 152.09, 152.43, 154.15, 156.36, 159.94. MS (ESI+) *m/z*: 357.3 (100%) (M + H). Anal. calcd for $C_{22}H_{20}N_4O$. 0.1H_2O: C, 73.76; H, 5.68; N, 15.64. Found C, 73.62; H, 5.39; N, 15.41.

3.2 Biological evaluation

3.2.1 Cell culture.
Human hepatocellular carcinoma (HCC) cell lines Huh7, HepG2, Hep3B, PLC, FOCUS, and Mahlavu, and breast (MCF7) and colon (HCT116) cancer cells were grown in Dulbecco's modified Eagle medium (DMEM) (Invitrogen GIBCO). The other HCC cell lines Snu182, Snu387, Snu398, Snu423, Snu449, and Snu475 were grown in RPMI-1640 (Invitrogen GIBCO) growth medium. All growth media were containing 1% penicillin/streptomycin(Invitrogen GIBCO), 1% non-essential amino acids (Lonza), and 10% fetal bovine serum (FBS) (Invitrogen GIBCO). All the cell lines were incubated at 37 °C with 5% CO_2.

3.2.2 Cytotoxicity screening with NCI-sulforhodamine B assay.
Human hepatocellular carcinoma (HCC) cell lines (Huh7, HepG2, Hep3B, PLC, FOCUS, Mahlavu, Snu182, Snu387, Snu398, Snu423, Snu449, and Snu475), and breast (MCF7) and colon (HCT116) cancer cell lines were inoculated into 96-well plates as 1000–3000 cells per well. After 24 h incubation, cells were treated with the compounds in

increasing concentrations (2.5–40 μM). Each and every drug treatment was performed in duplicate or triplicate. Fludarabine (Santa Cruz), cladribine (Santa Cruz), pentostatine (Santa Cruz), 5-fluorouracil (Kocak Farma) were used as positive controls, and DMSO (Sigma) was used as a negative control. After 72 h of incubation, the medium was discarded, and plates were washed twice with 1× PBS. Then the cells were fixed with 10% (w/v) trichloroacetic acid (TCA) (MERCK) solution for 1 h in the dark at +4 °C. In order to remove TCA, cells were then washed with ddH$_2$O about 4–5 times and left to air-dry at room temperature. The plates were then stained using 0.4% sulforhodamine B (SRB) (Sigma) solution in 1% acetic acid and incubated in the dark at room temperature for 10 min. Finally, the excess dye was discarded by washing off with 1% acetic acid 4–5 times until no dye came out and left to air dry at room temperature. Lastly, 10 mM cold TBS solution was used to solubilize the protein-bound SRB dye. Absorbance values were measured at 515 nm with a microplate reader. In order to calculate IC$_{50}$ values, the recorded OD value for each well was normalized to the OD value of its corresponding DMSO control.

3.2.3 Real-time cell electronic sensing for cell growth and cytotoxicity analysis. In order to assess the cytotoxic effect of the compounds in real-time, a real-time cell electronic sensing (RT-CES) (ACEA) system was used. Huh7 cells were seeded into E-plates in 100 μl growth medium as 2000 cells per well. After 24 h, cells were treated with the compound of interest and corresponding DMSO control, serving as a negative control. Cell index (CI) values were detected with 30 min intervals depicted from impedance measurements and reflected the cell growth.

3.2.4 Hoechst nuclei staining. Huh7 liver cancer cells were cultured in 6-well plates on coverslips as 50 000 cells per well. 24 h later, the growth medium was replaced with a fresh medium containing the compound of interest (5 μM) and its corresponding DMSO control. After 72 h of incubation, cells were washed twice with ice-cold 1× PBS. In order to permeabilize the cells, 100% ice-cold methanol was used for 10 min. Next, samples were washed with ice-cold 1× PBS once and stained with Hoechst 33258 stain (Sigma) for 5 min in the dark. Subsequently, the excess stain was discarded by washing with ddH$_2$O for 10 min on a shaker. Stained cells were then observed under a fluorescence microscope, and the images were captured using the ZEISS AxioCam MRc5 camera.

3.2.5 Cell cycle analysis using flow cytometry. Huh7 and Mahlavu cell lines were cultured into 100 mm culture dishes as 150 000–300 000 cells per well. 24 h later, the growth medium was aspirated, cells were washed twice with 1× PBS, and a fresh medium containing 1× FBS was placed to achieve starvation conditions to synchronize the cells. After an additional 24 h, a fresh growth medium containing the compound of interest and its corresponding DMSO control was replaced. After 72 h incubation period, cells were collected by trypsinization. The cell suspension was then centrifuged at 2000 rpm for 8 min. The supernatant was

discarded, and the cell pellet was re-suspended in 5 ml 1× PBS. The samples were again centrifuged at 2000 rpm for 8 min. Finally, the supernatant was discarded, and 50 μl 1× PBS was added for every 1 × 10^6 cells. Then 1 ml ice-cold 70% ethanol was added dropwise while vortexing at medium speed, and the samples were kept for at least 3 hours at −20 °C. Then the samples were stained with propidium iodide according to the manufacturer's protocol of the MUSE cell cycle kit (MCH100106, Millipore) and analyzed eventually.

3.2.6 Western blot analysis. Huh7 cells were inoculated into 100 mm culture dishes as 300 000 cells per well. 24 h later, the cells were treated with the selected compounds of interest (5 μM) and their corresponding DMSO controls. At the end of the 72 h incubation period, cells were collected with trypsin and incubated in lysis buffer (150 mM NaCl, 50 mM Tris-HCl pH = 7.6, 1% NP40, 0.1% SDS, 1× protease inhibitor cocktail, and 1× PhosStop). Purified proteins were quantified with Bradford and analyzed using antibodies against PARP-1 (Cell Signaling 9532), phospho-Src (Tyr416) (Santa Cruz sc10182), src (Santa Cruz sc19), Rb (Santa Cruz sc102), phospho-Rb (Ser807/811) (Cell Signaling 9308S), and Cdk2 (Santa Cruz sc6248). Calnexin (Sigma, C4731) and actin (Santa Cruz sc1616) were used for equal loading control. Secondary antibodies anti-mouse (Sigma, A0168) and anti-rabbit (Sigma, A6154) were used.

3.2.7 Kinase assay. Human liver cancer cells (Huh7 and Mahlavu) were grown in 100 mm culture dishes for 24 h as 150 000–300 000 cells per well. Then the cells were treated with the compounds of interest (5 μM) for 72 h. Following the lysis of the samples, a Bradford assay was used to determine the protein amount of each cell lysate. The Kinase Glo Plus luminescent kinase assay (Promega VC3772) kit was used according to the manufacturer's protocol to investigate the effect of the compounds of interest on kinase activity. Staurosporine (STR) (Calbiochem) was used as the positive control, and DMSO as the negative control of the assay.

3.2.8 KINOMEscan™ profiling of the compounds. The DMSO dissolved compounds of interest were sent to KINOMEscan™ where they were screened against a panel of human kinases to detect any possible direct interaction. The KINOMEscan™ scores for the test compounds initially dissolved in DMSO were calculated by taking DMSO as the negative control of the analysis.

3.3 Molecular modeling and molecular dynamics simulations

In the modeling step, there are two sets of molecules: small molecules to be tested and kinases as their target proteins. For the small molecule preparation, the three-dimensional (3D) structure of the purine analog compounds is drawn using ChemDraw. As reference molecules, anticancer agents fludarabine, 5-FU, pentostatine, and STR are also added to the small molecule library, and their structures were obtained from the Drugbank.[41] X-ray structures of the target kinases were also obtained from the Protein Data Bank.[29]

Molecular docking was performed using Autodock Vina[42,43] and the Chimera software[44] to optimize the synthesized compound's geometry and investigate the compounds' binding energy. Amber ff14SB and AM1-BCC force fields were applied to add charges in AmberTools.[45] The grid box size was set to 20 × 20 × 20 Å. The maximum number of binding modes and the maximum energy difference between modes were set to 20 kcal mol^{-1} and 10 kcal mol^{-1}, respectively, with an exhaustive global search of 32. After the molecular docking step, the protein–ligand interaction profiler (PLIP)[46] and the kinase database KLIFS[47] were used to analyze and visualize the interactions between the proteins and the small molecules. Finally, the resulting binding poses of AutoDock Vina are cross-checked with a second docking software, SwissDock.[48] In SwissDock, the accuracy mode with the grid box of 20 × 20 × 20 Å around the same center as AutoDock Vina was used with 250 poses for each target. Finally, the best-scored resulting poses are compared with the resulting poses of Autodock Vina.

Additionally, final poses are checked with molecular dynamics simulations for the stability of the poses of the small molecules inside the binding pocket. However, three X-ray structures of the target kinases had some missing loops. Therefore, GalaxyFill[49] was used to reconstruct remaining missing loops during MD preparation with CHARMM-GUI.[50] The protein systems were solvated in TIP3P water box sufficient in size to have at least 10 Å of water between the solute and the simulation box edges.[50–52] The complexes were neutralized with K$^+$ and Cl$^-$ (concentration: 0.15 mol L^{-1} KCl). For each simulation, an equilibration and ensuing 10 ns MD simulation were performed according to the protocol below. Initially, the system with the aqueous solvent environment was relaxed by performing a phase energy minimization over 10 000 steps. The system that was minimized was subsequently heated from 0 to 310.15 K, with positional restraints (1 kcal mol^{-1} Å^{-2}) applied to the kinase backbone and compound, lasting 0.25 ns. Then, simulations were run with periodic boundary conditions for 10 ns, at a constant temperature of 310.15 K, and 1 atm pressure (NPT) without any restraints. For the constant temperature control, Langevin dynamics was selected with the SHAKE algorithm for constrained hydrogen atoms. All MD simulations were performed using NAMD[53] with the CHARMM36m force field.[54] Visual molecular dynamics (VMD)[55] was used for root mean square deviation (RMSD) analysis.

4. Conclusions

In conclusion, nucleobase and nucleoside analogs have been used in cancer treatments for a long time due to their fundamental roles in various cellular processes such as cell growth or proliferation.[56] Purine analogs are propitious therapeutic agents which have been frequently investigated as potential protein kinase inhibitors with anticancer activity. The inactivation of an aberrantly active component responsible for tumorigenesis is a promising strategy against cancer cell growth. In this research, purine nucleobase analogs **11–24** and **47–56** were newly synthesized and analyzed primarily on breast (MCF7), colon (HCT116), and liver (Huh7) cancer cells. At this step, 5-fluorouracil (5-FU), pentostatine, fludarabine, and cladribine were used as positive controls. Eleven of the compounds showed significant growth inhibitory effects, and these molecules had IC$_{50}$ values less than 10 μM. These promising compounds were analyzed against an enlarged HCC panel by SRB, and their cytotoxic effects were then confirmed with the RT-CES system in real time. Afterward, five of these eleven compounds, **19**, **21**, **22**, **23**, and **56**, were selected for further molecular analysis on liver cancer cells. Hoechst analysis displayed apoptosis-like morphological changes such as horse-shoe structures or condensed nuclei of the cancer cells treated with these selected compounds. Furthermore, FACS analysis revealed SubG1/G1 cell cycle arrest in the presence of these novel nucleobase analogs as supporting data for the induction of apoptosis. In order to confirm apoptosis as the type of cell death triggered by these compounds, the expression of the poly (ADP-ribose) polymerase (PARP-1), a 113 kDa nuclear protein, was checked and found to be cleaved into apoptotic fragments. All the results correlate and verify that these novel purine analogs induce liver cancer cells to apoptosis. In order to clarify the underlying mechanism for this induction, further western blot analyses were performed. Compounds **19** and **23** were found to decrease the phospho-Src levels, briefly inhibiting the active form of Src protein. This inactivation affects the downstream elements cyclin E and cdk-2. Both downstream elements were confirmed to be inhibited in the presence of compounds **19** and **23**. Compared to its corresponding DMSO control, compound **19** also decreased the phospho-Rb levels. Consequently, newly synthesized novel urine nucleobase derivatives inhibit Src protein's phosphorylation, thus disrupting cyclin E and cdk2 complex formation. This complex would normally induce phosphorylation of Rb, which eventually inactivates Rb. In other words, the decrease in the phosphorylation of Rb, meaning its activation, was observed in compound **19** treated cells compared to its DMSO control (Fig. 8). The possible kinase inhibition potentials of these compounds were also investigated. Among all these nucleobase analogs, only compound **19** was shown to be a putative kinase inhibitor directly interacting with ALK and BTK. In anticancer drug discovery, both ALK and BTK are attractive targets due to their mutant forms that trigger cell growth and proliferation. Increased c-Src kinase activity is a common downstream effect of ALK and BTK activation. It is also known that BTK is an interaction partner of ALK, and its inhibition lessens the ischemia–reperfusion, causing hepatocellular damage. In this study, one of the newly synthesized purine analogs, compound **19**, was examined for its cytotoxic potential against a panel of liver cancer cell lines with IC$_{50}$ values less than 5 μM and the underlying mechanism that compound **19** utilizes to induce apoptosis *in vitro*.

Moreover, compounds **19**, **21**, **22**, **23**, and **56** are studied *in silico* by molecular docking together with STR and the other reference molecules. The binding affinities of all molecules showed better or similar values to STR with the target kinases. The binding poses are double checked with 10 ns molecular dynamics simulation of protein–compound complexes. In the final poses, compounds **19** and **56** both displayed very similar poses in the binding site of BTK, ALK, and DDR2, and this is a more extended pose compared to compounds **21**, **22**, and **23**. These molecules reach toward the front and back pockets as well as the activation loop. Activation loop interactions would bring inflexibility to the activation loop region. Finally, compound **19**, with BTK as its target kinase, displayed the most extended pose of the small molecule inside the active site by extending from the front to the back pocket through the gatekeeper region.

Author contributions

MT and RCA designed the study. EBG, IDS, DA, SE, and BS performed the study. MT, RCA, EBG, IDS, SE and BS analyzed the data. MT, EBG, IDS, SE and BS wrote the paper. All authors read and approved the manuscript.

Conflicts of interest

All authors declare that they have no conflict of interest.

Acknowledgements

References

1 J. Yin, W. Ren, X. Huang, J. Deng, T. Li and Y. Yin, *Front. Immunol.*, 2018, **9**, 1697.

2 A. M. Pedley and S. J. Benkovic, *Trends Biochem. Sci.*, 2017, **42**, 141–154.

3 E. Villa, E. S. Ali, U. Sahu and I. Ben-Sahra, *Cancers*, 2019, **11**, 688.

4 C. M. Galmarini, J. R. Mackey and C. Dumontet, *Lancet Oncol.*, 2002, **3**, 415–424.

5 W. B. Parker, *Chem. Rev.*, 2009, **109**, 2880–2893.

6 M. Legraverend and D. S. Grierson, *Bioorg. Med. Chem.*, 2006, **14**, 3987–4006.

7 P. Robak and T. Robak, *Cancer Treat. Rev.*, 2013, **39**, 851–861.

8 H. Sung, J. Ferlay, R. L. Siegel, M. Laversanne, I. Soerjomataram, A. Jemal and F. Bray, *Ca-Cancer J. Clin.*, 2021, **71**, 209–249.

9 R. L. Siegel, K. D. Miller, H. E. Fuchs and A. Jemal, *Ca-Cancer J. Clin.*, 2022, **72**, 7–33.

10 R. Kumari, M. K. Sahu, A. Tripathy, K. Uthansingh and M. Behera, *Hepatic Oncol.*, 2018, **5**, HEP08.

11 D. Marino, C. Zichi, M. Audisio, E. Sperti and M. Di Maio, *Drugs Context*, 2019, **8**, 212577.

12 F. Ma, Y. Zhu, X. Liu, Q. Zhou, X. Hong, C. Qu, X. Feng, Y. Zhang, Q. Ding, J. Zhao, J. Hou, M. Zhong, H. Zhuo, L. Zhong, Z. Ye, W. Xie, Y. Liu, Y. Xiong, H. Chen, D. Piao, B. Sun, Z. Gao, Q. Li, Z. Zhang, X. Qiu and Z. Zhang, *Hepatology*, 2019, **70**, 1785–1803.

13 R. B. Irby and T. J. Yeatman, *Oncogene*, 2000, **19**, 5636–5642.

14 T. Masaki, M. Okada, Y. Shiratori, W. Rengifo, K. Matsumoto, S. Maeda, N. Kato, F. Kanai, Y. Komatsu, M. Nishioka and M. Omata, *Hepatology*, 1998, **27**, 1257–1264.

15 I. Fabregat, *World J. Gastroenterol.*, 2009, **15**, 513–520.

16 E. N. De Toni, C. Kuntzen, A. L. Gerbes, W. E. Thasler, N. Sonuc, S. R. Mucha, P. Camaj, C. Bruns, B. Göke and S. T. Eichhorst, *J. Hepatol.*, 2007, **46**, 682–691.

17 X. Kong, P. Pan, H. Sun, H. Xia, X. Wang, Y. Li and T. Hou, *J. Med. Chem.*, 2019, **62**, 10927–10954.

18 T. Li, Y. Deng, Y. Shi, R. Tian, Y. Chen, L. Zou, J. U. Kazi, L. Rönnstrand, B. Feng, S. O. Chan, W. Y. Chan, J. Sun and H. Zhao, *Oncogene*, 2018, **37**, 6180–6194.

19 N. Maurya, R. Gujar, M. Gupta, V. Yadav, S. Verma and P. Sen, *J. Immunol.*, 2014, **193**, 3417–3425.

20 M. Tuncbilek, E. Bilget Guven, T. Onder and R. Cetin Atalay, *J. Med. Chem.*, 2012, **55**, 3058–3065.

21 M. Tuncbilek, A. Kucukdumlu, E. B. Guven, D. Altiparmak and R. Cetin-Atalay, *Bioorg. Med. Chem. Lett.*, 2018, **28**, 235–239.

22 A. Kucukdumlu, M. Tuncbilek, E. B. Guven and R. C. Atalay, *Acta Chim. Slov.*, 2020, **67**, 70–82.

23 A. Kucukdumlu, M. Tuncbilek, E. B. Guven and R. C. Atalay, *Acta Chim. Slov.*, 2017, **64**, 621–632.

24 M. Tunçbilek, Z. Ateş-Alagöz, N. Altanlar, A. Karayel and S. Özbey, *Bioorg. Med. Chem.*, 2009, **17**, 1693–1700.

25 H. Huang, J. Ma, J. Shi, L. Meng, H. Jiang, J. Ding and H. Liu, *Bioorg. Med. Chem.*, 2010, **18**, 4615–4624.

26 T. Prathapam, S. Tegen, T. Oskarsson, A. Trumpp and G. S. Martin, *Proc. Natl. Acad. Sci. U. S. A.*, 2006, **103**, 2695–2700.

27 A. T. Bender, A. Gardberg, A. Pereira, T. Johnson, Y. Wu, R. Grenningloh, J. Head, F. Morandi, P. Haselmayer and L. Liu-Bujalski, *Mol. Pharmacol.*, 2017, **91**, 208–219.

28 M. Menichincheri, E. Ardini, P. Magnaghi, N. Avanzi, P. Banfi, R. Bossi, L. Buffa, G. Canevari, L. Ceriani, M. Colombo, L. Corti, D. Donati, M. Fasolini, E. Felder, C. Fiorelli, F. Fiorentini, A. Galvani, A. Isacchi, A. L. Borgia, C. Marchionni, M. Nesi, C. Orrenius, A. Panzeri, E. Pesenti, L. Rusconi, M. B. Saccardo, E. Vanotti, E. Perrone and P. Orsini, *J. Med. Chem.*, 2016, **59**, 3392–3408.

29 H. M. Berman, *Nucleic Acids Res.*, 2000, **28**, 235–242.

30 J. N. Zambrano, C. J. Williams, C. B. Williams, L. Hedgepeth, P. Burger, T. Dilday, S. T. Eblen, K. Armeson, E. G. Hill and E. S. Yeh, *Oncotarget*, 2018, **9**, 35962–35973.

31 K. Sasaki, T. Tsukada, I. Adachi and K. Yamaguchi, *Biochem. Biophys. Res. Commun.*, 1995, **214**, 1114–1120.

32 P. M.-U. Ung and A. Schlessinger, *ACS Chem. Biol.*, 2015, **10**, 269–278.

33 R. Roskoski, *Pharmacol. Res.*, 2016, **103**, 26–48.

34 V. Modi and R. L. Dunbrack, *Proc. Natl. Acad. Sci. U. S. A.*, 2019, **116**, 6818–6827.

35 R. V. Patel, B. M. Mistry, R. Syed, N. M. Parekh and H. S. Shin, *Arch. Pharm.*, 2019, **352**, e1900051.

36 A. H. Channigarayappa, S. Swamy, M. R. Nadigar, V. Chandramohan and S. Govindaiaha, *Asian J. Pharm. Pharmacol.*, 2017, **3**, 177–185.

37 G. X. Zhu, P. Le Cheng, M. Goto, N. Zhang, S. L. Morris-Natschke, K. Y. Hsieh, G. Z. Yang, Q. R. Yang, Y. Q. Liu, H. Le Chen, X. S. Zhang and K. H. Lee, *Bioorg. Med. Chem. Lett.*, 2017, **27**, 1750–1753.

38 L. Chen, H. Chen, P. Chen, W. Zhang, C. Wu, C. Sun, W. Luo, L. Zheng, Z. Liu and G. Liang, *Eur. J. Med. Chem.*, 2019, **161**, 22–38.

39 N. R. Kode and S. Phadtare, *Molecules*, 2011, **16**, 5840–5860.

40 C. A. Fleckenstein and H. Plenio, *Chem. – Eur. J.*, 2008, **14**, 4267–4279.

41 D. S. Wishart, Y. D. Feunang, A. C. Guo, E. J. Lo, A. Marcu, J. R. Grant, T. Sajed, D. Johnson, C. Li, Z. Sayeeda, N. Assempour, I. Iynkkaran, Y. Liu, A. Maciejewski, N. Gale, A. Wilson, L. Chin, R. Cummings, D. Le, A. Pon, C. Knox and M. Wilson, *Nucleic Acids Res.*, 2018, **46**, D1074–D1082.

42 O. Trott and A. J. Olson, *J. Comput. Chem.*, 2010, **31**, 455–461.

43 J. Eberhardt, D. Santos-Martins, A. F. Tillack and S. Forli, *J. Chem. Inf. Model.*, 2021, **61**, 3891–3898.

44 E. F. Pettersen, T. D. Goddard, C. C. Huang, G. S. Couch, D. M. Greenblatt, E. C. Meng and T. E. Ferrin, *J. Comput. Chem.*, 2004, **25**, 1605–1612.

45 D. A. Case, H. M. Aktulga, K. Belfon, D. S. Cerutti, G. A. Cisneros, V. W. D. Cruzeiro, N. Forouzesh, T. J. Giese, A. W. Götz, H. Gohlke, S. Izadi, K. Kasavajhala, M. C. Kaymak, E. King, T. Kurtzman, T. S. Lee, P. Li, J. Liu, T. Luchko, R. Luo and K. M. Merz Jr., *J. Chem. Inf. Model.*, 2023, **63**, 6183–6191.

46 M. F. Adasme, K. L. Linnemann, S. N. Bolz, F. Kaiser, S. Salentin, V. J. Haupt and M. Schroeder, *Nucleic Acids Res.*, 2021, **49**, W530–W534.

47 O. P. J. van Linden, A. J. Kooistra, R. Leurs, I. J. P. de Esch and C. de Graaf, *J. Med. Chem.*, 2014, **57**, 249–277.

48 A. Grosdidier, V. Zoete and O. Michielin, *Nucleic Acids Res.*, 2011, **39**, W270–W277.

49 E. A. Coutsias, C. Seok, M. P. Jacobson and K. A. Dill, *J. Comput. Chem.*, 2004, **25**, 510–528.

50 S. Jo, T. Kim, V. G. Iyer and W. Im, *J. Comput. Chem.*, 2008, **29**, 1859–1865.

51 J. Lee, X. Cheng, J. M. Swails, M. S. Yeom, P. K. Eastman, J. A. Lemkul, S. Wei, J. Buckner, J. C. Jeong, Y. Qi, S. Jo, V. S. Pande, D. A. Case, C. L. Brooks, A. D. MacKerell, J. B. Klauda and W. Im, *J. Chem. Theory Comput.*, 2016, **12**, 405–413.

52 J. Lee, M. Hitzenberger, M. Rieger, N. R. Kern, M. Zacharias and W. Im, *J. Chem. Phys.*, 2020, **153**, 035103.

53 J. C. Phillips, R. Braun, W. Wang, J. Gumbart, E. Tajkhorshid, E. Villa, C. Chipot, R. D. Skeel, L. Kalé and K. Schulten, *J. Comput. Chem.*, 2005, **26**, 1781–1802.

54 K. Vanommeslaeghe and A. D. MacKerell, *Biochim. Biophys. Acta*, 2015, **1850**, 861–871.

55 W. Humphrey, A. Dalke and K. Schulten, *J. Mol. Graphics*, 1996, **14**, 33–38.

56 P. Karran, *Br. Med. Bull.*, 2007, **79–80**, 153–170.